

# Agents-K1: Towards Agent-native Knowledge Orchestration

Zongsheng Cao<sup>\*</sup>, Bihao Zhan<sup>\*,\*</sup>, Jinxin Shi<sup>\*,\*</sup>, Jiong Wang<sup>\*,\*</sup>, Fangchen Yu<sup>\*</sup>, Zhijie Zhong<sup>\*</sup>, Zijie Guo<sup>\*,\*</sup>, Tianshuo Peng<sup>\*</sup>, Zhuo Liu<sup>\*</sup>, Yi Xie<sup>\*</sup>, Xiang Zhuang<sup>\*</sup>, Yue Fan<sup>\*</sup>, Runmin Ma<sup>\*</sup>, Shiyang Feng<sup>\*</sup>, Xiangchao Yan<sup>\*</sup>, Anran Liu<sup>\*</sup>, Peng Ye<sup>\*</sup>, Wenlong Zhang<sup>\*</sup>, Shufei Zhang<sup>\*</sup>, Chunfeng Song<sup>\*</sup>, Fenghua Ling<sup>\*</sup>, Jie Zhou<sup>\*,\*</sup>, Liang He<sup>\*,\*</sup>, Bo Zhang<sup>\*,\*</sup>, Lei Bai<sup>\*,\*</sup>

<sup>\*</sup>Shanghai Artificial Intelligence Laboratory, <sup>\*</sup>East China Normal University, <sup>◇</sup>Fudan University

**Abstract** Current LLM-based research agents have advanced through agent orchestration, yet largely overlook scientific knowledge orchestration. Existing works often reduce papers to abstracts, surface mentions, and flat cites edges, omitting key entities, claims, evidence, mechanisms, and method lineages essential for scientific reasoning. To this end, we introduce **Agents-K1**, an end-to-end knowledge orchestration pipeline that converts raw documents into agent-native scientific knowledge graphs. Agents-K1 integrates three components under a unifying theoretical foundation: a multimodal parser whose five-module schema captures entities, multimodal evidence, citations, and typed inter-entity relations across the full paper rather than abstracts alone; a 4B information-extraction backbone trained with GRPO under a rule-based reward; and a graphanything CLI, a tri-source agent interface that unifies web search, multimodal graph retrieval, and cross-document traversal. On top of this, we process 2.46 million scientific papers across six subjects to produce **Scholar-KG**, of which we release a one-million-paper subset, and the full Scholar-KG is accessible via the SCP link below. The same pipeline can be extended to general-domain corpora and to schema-conformant data synthesis. Extensive experiments demonstrate that Agents-K1 achieves superior performance in scientific information extraction, knowledge graph construction, and multi-hop scientific reasoning.

SCP Code Data Model

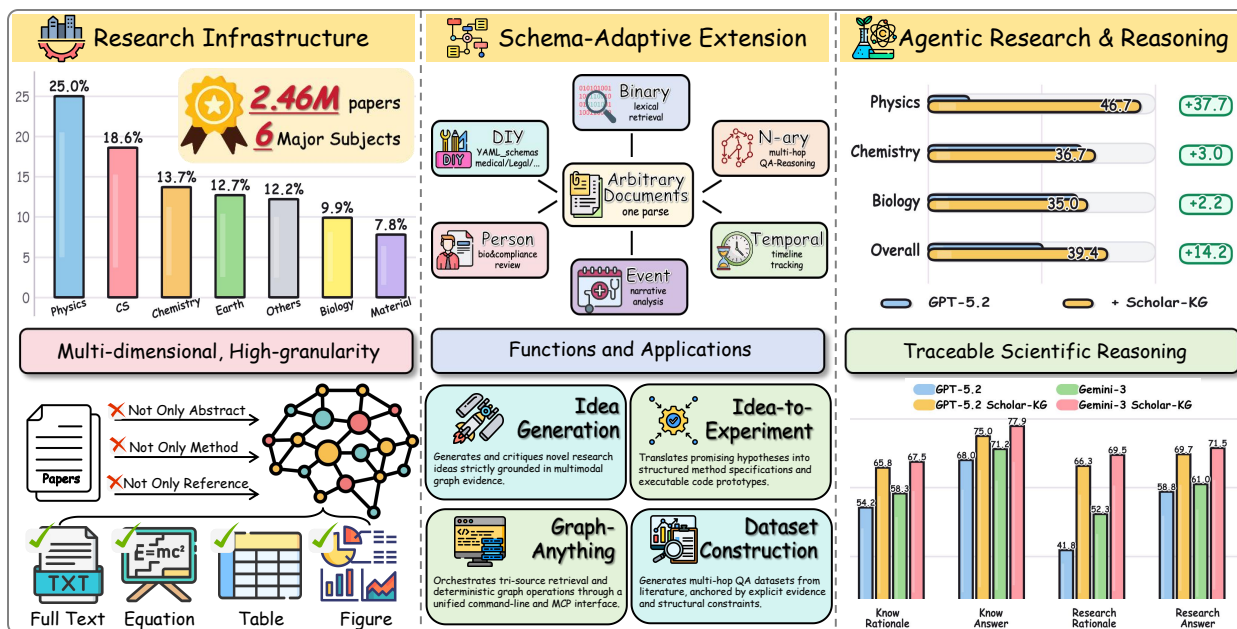


Figure 1 | **Agents-K1: Architecture and Capabilities.** **Left:** Extracting multimodal knowledge from scientific papers. **Middle:** Schema-adaptive extensions for core research tasks. **Right:** Enhancing LLM reasoning and verifiable knowledge tracing.

# Contents

<b>1</b>	<b>Introduction</b>	<b>3</b>
<b>2</b>	<b>Related Work</b>	<b>4</b>
<b>3</b>	<b>The Overall Agents-K1 Framework</b>	<b>6</b>
<b>4</b>	<b>KG Layer: An end-to-end Pipeline for Scientific Knowledge Construction</b>	<b>7</b>
4.1	Scientific Knowledge Network Construction	8
4.2	Dataset Construction via LLM-Guided Multi-Hop QA Generation.	11
4.3	General-KG: A Multi-View, Schema-Adaptive Extension to Arbitrary Documents	12
4.4	Knowledge Organization and Storage	15
4.5	Theoretical Foundations	15
<b>5</b>	<b>LLM Layer: Reinforcement-Learned Information Extraction Backbone</b>	<b>17</b>
5.1	Training Algorithm	17
5.2	Reward Function	17
<b>6</b>	<b>CLI Layer: A Knowledge-Grounded Multi-Agent Research Toolkit</b>	<b>18</b>
6.1	Tri-Source Knowledge Retrieval and Fusion	19
6.2	Graph Operators and Multi-Agent Coordination	20
6.3	Idea-to-Experiment Pipeline	22
6.4	Downstream Tasks and Examples	24
<b>7</b>	<b>Experiments</b>	<b>25</b>
7.1	Domain Distribution and Coverage	25
7.2	Evaluation Metrics	26
7.2.1	Metric Formulations	26
7.2.2	Semantic-Aware Evaluation Criteria	26
7.3	Cross-Domain Performance Analysis	27
7.4	Performance Comparison on Knowledgeable and Research Questions	29
7.5	Performance on open source benchmarks	31
7.5.1	Datasets and Evaluation Metrics	31
7.5.2	Baselines	31
7.5.3	Results and Analysis	32
7.6	Information Extraction Backbone Evaluation	33
7.6.1	Setup	33
7.6.2	Main Results	33
<b>8</b>	<b>Conclusion</b>	<b>34</b>
	<b>References</b>	<b>35</b>
	<b>Appendix</b>	<b>38</b>
A	Citation Context Classification Schema	38
B	Proofs and Constructive Details for Section 4.5	38
B.1	Projection Rules	38
B.2	Proof of Proposition 1 (Identifier Preserving Joins)	39
B.3	Proof of Proposition 2 (Cross View Reachability)	39
B.4	Proof of Proposition 3 (Candidate Coverage)	40
B.5	Witness Construction for the Strict-Gap Term	40
C	Knowledge Graph Visualization	40
D	Disaggregated Knowledge Graph Schema	42

## 1. Introduction

LLM-based research agents have moved from prototype to deployment over the past two years. Advanced systems such as AI-Scientist [1], InternAgent [2, 3], and AI Co-Scientist [4] can now plan experiments, retrieve literature, write code, and draft papers in a single loop. Specifically, their progress depends on two parts: *agent orchestration*, which decides how agents plan and act, and *knowledge orchestration*, which decides what knowledge they can use and how that knowledge is organized. Most recent work has focused on agent orchestration. The knowledge counterpart, however, remains much less developed.

This gap matters because a research agent needs more than a list of relevant papers. It needs structured knowledge that preserves what each paper claims, what evidence supports the claim, how the claim relates to prior work, and where the evidence can be checked. Current scientific knowledge infrastructure falls short of this requirement in three ways. First, modern graph-augmented retrieval pipelines, including LightRAG [5], HippoRAG [6], HippoRAG2 [7], GFM-RAG [8], E<sup>2</sup>GraphRAG [9], RAPTOR [10], and KGP [11], usually build generic text-only triples. They capture little beyond abstracts and directly mentioned terms, so key entities, claims, mechanisms, and method links remain buried in the full paper. Figures, tables, and equations, which often carry key evidence, are usually reduced to captions. Second, scholarly citation graphs usually use a flat `cites` edge. This shows that one paper references another, but not whether it extends a method, challenges a claim, or only cites a baseline. Third, LLM-based research agents [1, 3, 4] often read raw PDFs or short summaries at runtime. This repeats extraction for each query and makes it hard to trace an answer back to exact evidence. These limitations are not just retrieval errors; they show that the knowledge infrastructure itself is not yet designed for agent reasoning.

These limitations point to a different design goal: agent-native *knowledge orchestration*. It should meet three requirements. First, it should cover the full paper and treat text, figures, tables, and equations as connected evidence rather than separate artifacts. Second, it should turn scientific content into typed knowledge, including entities, claims, mechanisms, method links, citation roles, and inter-entity relations. Third, it should support auditable retrieval, so that an agent can trace each answer or decision back to stable graph identifiers and exact evidence. Meeting these requirements calls for a unified pipeline that combines full-paper graph construction, affordable structured extraction, and an agent-facing retrieval interface. This raises a natural question: *Can we build such a unified pipeline to turn raw scientific papers into agent-ready scientific knowledge graphs and support reliable research-agent reasoning at scale?*

To this end, we present **Agents-K1**, an end-to-end knowledge orchestration pipeline that converts raw documents into agent-native multimodal knowledge graphs at scale. Agents-K1 integrates a multimodal parser, a five-module extraction schema, a reinforcement-learned extraction model, and a tri-source agent CLI into a single framework, and the same pipeline can be replayed on arbitrary corpora. The first stage is multimodal parsing and schema (Section 4). It uses a MinerU-based offline parser to ingest PDFs and a five-module schema (metadata, explicit mentions, implicit abstractions, citation intent, and fine-grained inter-entity relations) that organises the entire paper rather than its abstract alone, with figures, tables, and equations admitted as first-class evidence alongside textual entities. The second stage is the extraction backbone (Section 5). It is a 4B-parameter model trained with Group Relative Policy Optimization and a rule-based reward jointly supervising format compliance, JSON validity, and task-conditioned F1 on named entity recognition, relation extraction, and long-form structured extraction. It surpasses an 8B open-source reference across ten benchmarks and matches a 32B base on NER while remaining inexpensive to retrain on new domains. The third stage is the agent CLI (Section 6). It fuses real-time web search, multimodal graph retrieval, and cross-document network traversal into a single tri-source interface and orchestrates a closed-loop workflow

of idea generation, method specification, and code synthesis. On the FRONTIERSCIENCE-RESEARCH benchmark [12], it lifts Gemini-3 overall accuracy from 7.9% to 24.6% and GPT-5.2 from 25.2% to 39.4%; on geoscience research questions, it lifts Gemini-3 rationale accuracy from 52.3% to 69.5%; and on multi-hop QA, it reaches state-of-the-art performance on HotpotQA [13], 2WikiMultiHopQA [14], and MuSiQue [15] against nine graph-augmented retrieval baselines. Theoretical analysis further supports this design by explaining why organizing evidence in one connected graph makes cross-source reasoning more reliable than searching separate text fragments.

We instantiate Agents-K1 on scientific literature by processing 2.46 million papers across six disciplines (computer science, chemistry, biology, earth science, physics, and materials) to produce **Scholar-KG**, and release a one-million-paper subset for community research. Beyond scientific papers, the same parser and extraction backbone can be retargeted through a schema-adaptive variant to build **General-KG** over arbitrary document corpora, without bespoke per-domain engineering. The structured JSON outputs can also serve as schema-conformant data for training downstream extraction and reasoning models.

The main contributions of this paper are summarised as follows.

- **Unified scientific knowledge infrastructure.** We introduce **Agents-K1**, an agent-native knowledge orchestration pipeline that unifies KG, LLM, and CLI in a unified framework. Unlike static scholarly knowledge graphs, Agents-K1 is designed around the full workflow of research agents: parsing papers, extracting structured knowledge, building reusable graphs, and exposing the resulting knowledge through agent-facing interfaces.
- **Million-scale full-paper multimodal knowledge graphs.** Agents-K1 constructs **Scholar-KG** from 2.46 million scientific papers across six disciplines, with a one-million-paper subset released for community research. The pipeline models the full paper rather than only titles, abstracts, metadata, or citation graphs, extracting entities, claims, evidence, motivations, mechanisms, method lineages, citation intent, and inter-entity relations.
- **Reinforcement-learned extraction backbone.** We train a 4B-parameter information-extraction model with GRPO and a rule-based reward that jointly supervises format compliance, JSON validity, and task-conditioned F1 on NER, relation extraction, and long-form structured extraction.
- **GraphAnything CLI for executable graph-based research.** We provide GraphAnything CLI as an agent-facing interface that turns the graph from a static data asset into an executable research tool. It supports web search, multimodal graph retrieval, cross-document traversal, graph operations, and graph evolution through CLI/MCP/API access, enabling research agents to directly use the graph in end-to-end research workflows.

## 2. Related Work

**Retrieval-Augmented Generation.** As AI systems are increasingly expected to solve knowledge-intensive tasks [16, 17, 18], Retrieval-Augmented Generation (RAG) [19, 20] has become an important paradigm for extending large language models (LLMs) beyond their internal parametric knowledge. Instead of relying solely on information memorized during pretraining, RAG introduces an external knowledge source into the generation pipeline. In general, it first organizes documents or data into a retrievable knowledge base, then identifies evidence relevant to a given query, and finally conditions the LLM on the retrieved content to support generation and reasoning. By allowing models to access fresh, domain-specific, and task-related information, RAG significantly improves their ability to produce responses that are both factually grounded and contextually appropriate [21, 22]. This makes RAG especially suitable for real-world scenarios where accurate knowledge access and reliable reasoning are required at the same time.

Existing RAG studies have developed along multiple directions, mainly driven by the need to handle increasingly complex knowledge sources. Chunk-based retrieval methods [16, 23, 24] focus on dividing documents into effective retrieval units and improving the matching between queries and textual segments through better embeddings and segmentation strategies. In contrast, graph-based RAG systems [25, 21, 26] attempt to move beyond independent text chunks by introducing explicit relational structures, thereby enabling models to retrieve and reason over connected knowledge more effectively. Meanwhile, multimodal RAG [27] further expands the retrieval space beyond plain text to heterogeneous information such as images, audio, and video, enabling richer evidence integration across modalities and application settings.

**Graph-based Information Understanding.** To provide more structured supporting evidence for LLM reasoning, GraphRAG [25] marks a representative step toward incorporating knowledge graph structures [28] into retrieval-augmented generation. Following this line of work, many approaches [29, 30, 31, 32, 33] have adapted graph-based RAG frameworks to different domains and tasks, showing that graph structures can improve how external knowledge is organized, retrieved, and used by LLMs. For example, LightRAG [21] enhances retrieval efficiency by introducing graph indexing and update mechanisms, while PathRAG [34] and HippoRAG2 [35] further improve graph retrieval through path pruning and Personalized PageRank, respectively. Nevertheless, the effectiveness of these methods is still largely constrained by how the graph itself is constructed. Most existing graph-based RAG approaches mainly extract knowledge from textual content and encode it as fragmented triples or other local relational units. Although such representations are useful for capturing isolated facts, they often lose the broader semantic continuity of the original corpus, especially when the source documents contain complex structures, long-range dependencies, figures, tables, and hierarchical arguments. As a result, the constructed graphs may fail to reflect the complete information organization of papers and other knowledge-intensive corpora. This motivates the need for an end-to-end information extraction method that can model document-level knowledge more comprehensively and preserve richer semantic relations during graph construction.

**Deep Research Agents.** The Deep Research Agents [36, 37, 38, 39, 40] advance a long-horizon research paradigm for knowledge-intensive tasks. A typical system follows a recurring loop of planning, retrieval, reading, verification, and re-retrieval, which autonomously fills knowledge gaps and progressively reduces uncertainty. Both OpenAI [41] and Gemini [42] emphasize first constructing an adaptable research plan around a complex question, then conducting multiple rounds of exploration and cross-validation across heterogeneous sources to support deeper, research-oriented problem-solving. Another line of work focuses on dynamic reasoning and tool use. For example, InternAgent [2, 3] and WebThinker [39] make deep research explicit as continual search and information extraction, and improve tool-use quality via preference optimization. Complementary to multi-agent paradigms, the single-agent direction also evolves rapidly. Tongyi DR [38] trains a self-regulated reasoning agent with reinforcement learning to learn action selection.

However, most existing solutions still treat webpages or plain-text retrieval as the primary gateway to knowledge, making it difficult to fully exploit key evidence in scientific literature carried by figures, tables, and formulas. In contrast, this paper uses semantic anchors to integrate text, images, tables, and formulas into a unified, retrievable knowledge representation and to fuse three sources: web retrieval, multimodal knowledge graph retrieval, and cross-paper knowledge network traversal. This design provides a more structure-aware and evidence-traceable knowledge infrastructure for deep research workflows, reduces information blind spots caused by text-centric retrieval, and opens a new path to better control the solution space and improve reproducibility.

### 3. The Overall Agents-K1 Framework

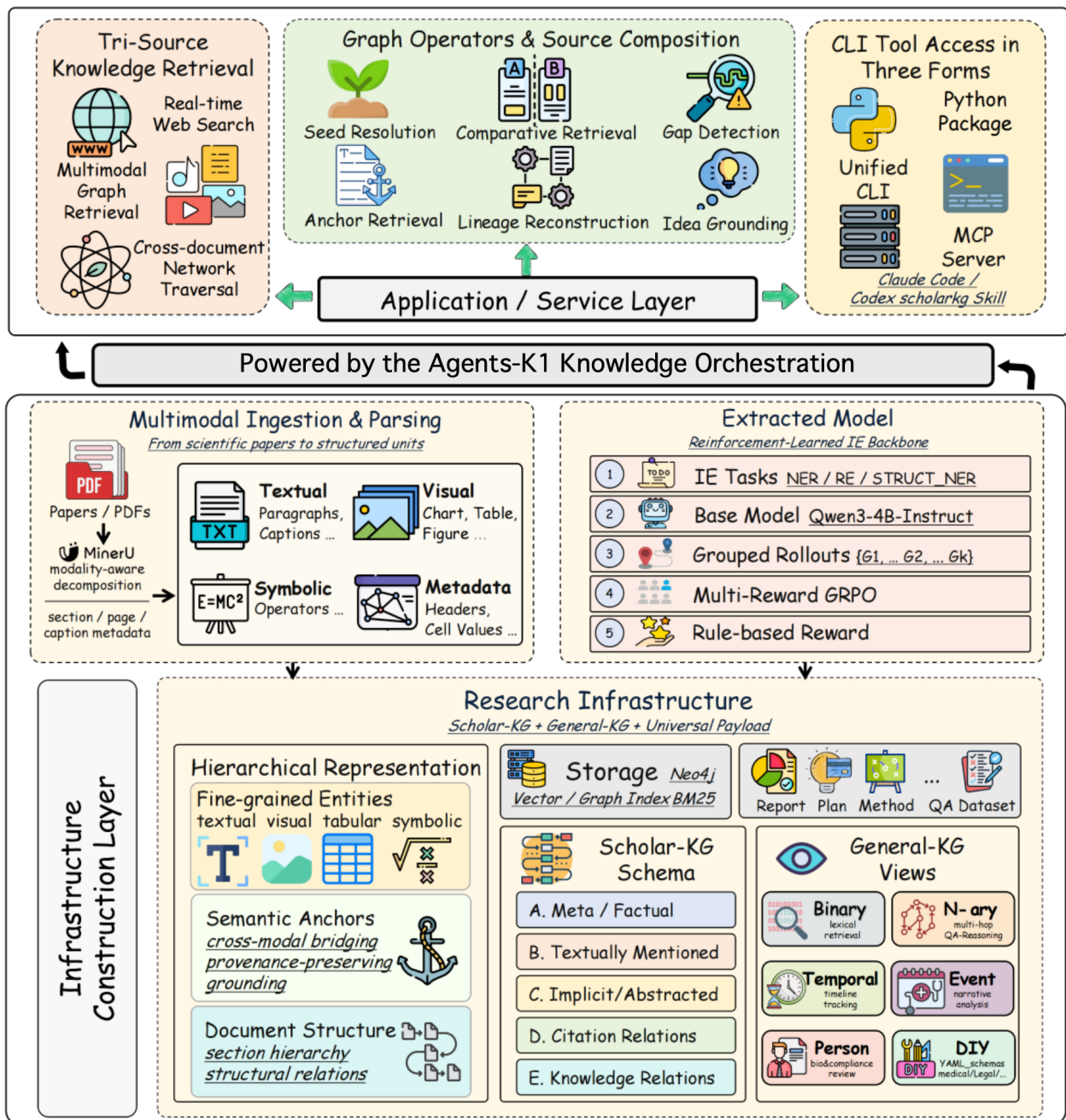


Figure 2 | Overall framework of Agents-K1. Agents-K1 features three parts. The **infrastructure construction layer** parses multimodal documents into structured knowledge graphs (Scholar-KG and General-KG). Utilizing this foundation, the **application/service layer** offers a **tri-source agent CLI** as the main interface, enabling comprehensive and auditable research workflows such as comparative analysis and idea grounding.

Scientific research agents need more than a powerful reasoning model. To answer complex research questions, an agent must identify relevant papers, inspect evidence across text, figures, tables, and equations, connect claims across documents, and keep the final answer traceable to its sources. However, many existing scholarly infrastructures expose only abstracts, metadata, and coarse citation

links. Important information such as methods, assumptions, evidence, limitations, and method lineages therefore remains buried in raw papers, forcing the agent to repeatedly recover this structure at query time.

Agents-K1 is designed as a reusable knowledge infrastructure for this setting. Instead of asking the agent to reason directly over scattered PDFs and flat search results, Agents-K1 first converts documents into structured multimodal knowledge graphs, then exposes these graphs through retrieval and tool interfaces that an agent can use during research. In this way, the framework separates two jobs that are often mixed together: offline construction of reliable knowledge representations, and online use of this knowledge for evidence-grounded reasoning.

As shown in Figure 2, Agents-K1 addresses this problem through three coordinated components. First, the KG layer (Section 4) parses the full paper rather than only the abstract, extracts multimodal content units, and organizes metadata, explicit concepts, implicit claims, citation intent, and fine-grained relations into graph structures. This produces **Scholar-KG** for scientific literature and extends to **General-KG** for other document collections through a schema-adaptive design. Second, the LLM layer (Section 5) supplies the extraction backbone used to populate these graphs. We train a compact 4B model with reinforcement learning and rule-based rewards so that large-scale extraction can remain accurate, structured, and affordable to adapt. Third, the agent CLI layer (Section 6) makes the constructed knowledge usable by research agents. Its tri-source CLI combines web search, multimodal graph retrieval, and cross-document traversal, allowing the agent to retrieve evidence, follow provenance, compare related works, and ground new ideas in existing literature.

#### 4. KG Layer: An end-to-end Pipeline for Scientific Knowledge Construction

A central challenge in scientific knowledge representation lies in bridging the semantic gap between heterogeneous content types. Traditional approaches either flatten all modalities into text (losing visual structure) or maintain separate representations (complicating cross-modal retrieval). We observe that scientific documents exhibit a natural hierarchical organization: fine-grained entities (methods, datasets, metrics) are semantically grounded within coarse-grained content units (figures, tables, paragraphs), which together compose the document’s narrative structure. This observation motivates our semantic anchor design, an intermediate abstraction layer that serves as modality-agnostic bridges, enabling entities from different modalities to connect through shared semantic anchors rather than requiring direct cross-modal alignment.

**Multimodal Content Decomposition** The first stage transforms raw documents into a canonical representation suitable for unified processing. Each knowledge source  $k_i \in \mathcal{K}$  undergoes modality-aware decomposition:

$$k_i \xrightarrow{\text{Parse}} C_i = \{c_j = (t_j, x_j, m_j)\}_{j=1}^{n_i}, \quad (1)$$

where each content unit  $c_j$  comprises a modality type  $t_j \in \{\text{text, figure, table, equation}\}$ , raw content  $x_j$ , and structural metadata  $m_j$  (e.g., section hierarchy, page location, caption associations). Specialized parsers handle each modality: text is segmented into semantically coherent paragraphs; figures are extracted with captions and cross-references; tables preserve cell structure with headers; equations retain symbolic representations alongside surrounding context. This decomposition maintains the document’s inherent organization while enabling modality-specific processing.

**Unified Heterogeneous Graph with Semantic Anchors.** For the given multimodal document, instead of constructing modality-specific graphs and aligning them post-hoc, we represent all multimodal content within a single heterogeneous graph  $\mathcal{G} = (\mathcal{V}, \mathcal{E}, \phi_v, \phi_e)$  organized into three layers. The lowest layer contains fine-grained entities extracted from text, figures, tables, and equations (e.g.,

named entities, visual concepts, table entries, symbolic variables). To avoid brittle cross-modal entity alignment, we introduce a middle semantic anchor layer: for each content unit  $c_j$ , we generate an abstract anchor node

$$a_j = f_{\text{MLLM}}(c_j, \mathcal{N}_j), \quad (2)$$

where  $\mathcal{N}_j$  provides local contextual grounding. Each anchor captures a modality-agnostic semantic summary together with salient entities and relations, serving as a stable bridge across modalities while preserving fine-grained provenance.

The top layer models document structure (sections and documents), enabling hierarchical retrieval and global context. Cross-layer edges link entities to anchors via `grounded_in` relations, and anchors to structure via `belongs_to` edges. Relationships among anchors are induced through explicit references, shared canonical entities, and semantic similarity in embedding space. By routing multimodal interactions through semantic anchors rather than direct entity matching, the graph achieves improved robustness and retrieval reliability while remaining lightweight and extensible.

#### 4.1. Scientific Knowledge Network Construction

To effectively utilize the abundant literature and papers, we collect them and leverage MinerU to conduct multimodal understanding. In this way, we construct a comprehensive scientific knowledge network that captures both explicit and implicit knowledge from research papers. This knowledge network serves as a structured repository that organizes entities, relationships, and scientific claims extracted from the literature, enabling efficient retrieval and reasoning for downstream applications. The network construction process involves defining a hierarchical schema, implementing multimodal knowledge extraction, and organizing the extracted knowledge into a queryable graph structure.

As shown in the Figure 3, our knowledge graph schema is designed to capture the multi-faceted nature of scientific literature, encompassing verifiable metadata, explicitly mentioned concepts, implicitly abstracted knowledge, and citation relationships. We organize entities into five categories:

**A. Meta/Factual Entities.** We define a stable backbone of low-variance, verifiable metadata that supports deduplication, disambiguation, and provenance across the corpus. For each Paper, we normalize title, doi/arXiv\_id, pub\_year, venue (conf/journal/workshop), type (long/short), language, peer\_review\_status, license, country/region, and resolvable pdf/supplement URLs. Authors are canonicalized (Surname, Given) with ORCID/email (hashed if required), ordered positions, corresponding flags, and linked Affiliations harmonized to ROR IDs with country and dept/lab fields. We capture process times (submission, accept, camera-ready) and open-science Resources, including repository URLs pinned to commits, model artifact hashes, and dataset releases with names/versions. Each field is stored with provenance  $\langle \text{doc}, \text{section/page}, \text{span} \rangle$  and a calibrated confidence score, providing a trustworthy spine for downstream reasoning and global entity linking.

**B. Textually Mentioned Entities.** We lift all explicitly referenced scientific objects into normalized nodes to enable high-precision retrieval and reproducible comparisons. Span detectors and sequence labelers identify noun phrases for *Tasks/Problems* (names, modalities, settings such as zero/few-shot and common aliases), *Methods/Models/Algorithms* (proposed/cited names, modular components like encoders/experts/routers, training objectives such as cross-entropy/KL/GRPO, and inference strategies), *Datasets/Splits/Modalities* (name, year/version, official splits, subsets, pre-processing such as tokenizers or image sizes), *Metrics* (long names, acronyms, formula semantics, macro/micro/weighted variants and alignment with official implementations, including deprecations like BLEU $\rightarrow$ ChrF), *Baselines* (versioned and tagged as official/reproduced/strong), *Implementation/-Training* details (framework, hardware and VRAM class, batch/lr/scheduler, epochs, seeds, AMP,

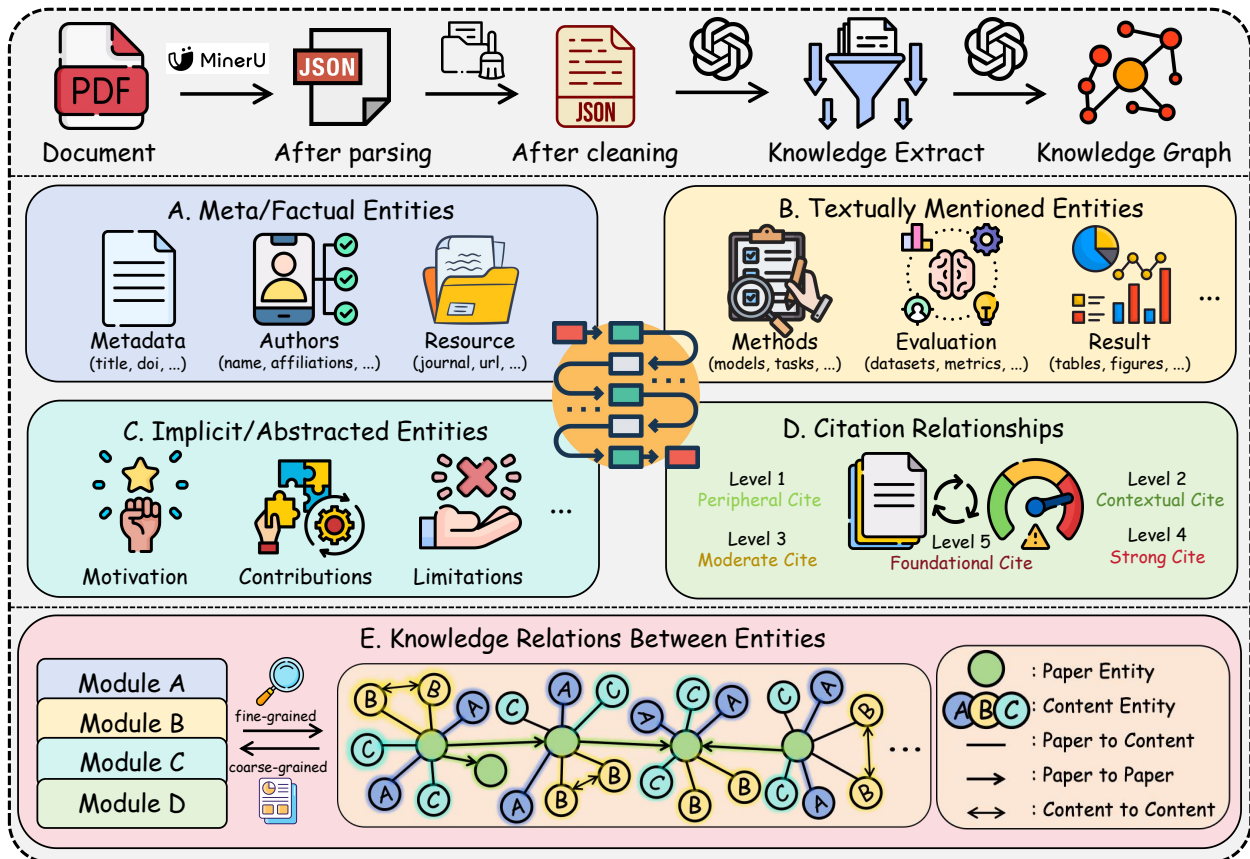


Figure 3 | Framework for Scientific Knowledge Network Construction. (a) Meta/factual entities provide a stable backbone for deduplication and provenance tracking through standardized metadata, author canonicalization, and resource linking. (b) Textually mentioned entities capture explicit scientific objects (methods, datasets, metrics) with synonym recognition and core-focus recall for fair benchmarking. (c) Implicit/abstracted entities synthesize high-level knowledge, including motivations, contributions, and limitations, through rhetorical-role tagging and discourse parsing. (d) Citation relationships encode argumentative intent (support/contrast/extend) and strength scores, enabling lineage tracing and causal mapping of claim propagation across the literature. (e) Knowledge relations between entities refine coarse abstractions into fine-grained, queryable triples, turning the graph into a navigable reasoning surface.

adapters, and toolchain such as Apex/Deepspeed/FlashAttn), formal *Theorems/Definitions/Lemmas* (IDs, premises, conclusions), and structured references to *Figures/Tables/Equations/Examples* (IDs, captions, page anchors). Mentions are canonicalized through controlled vocabularies and embedding-based entity linking into the ontology; all nodes carry evidence spans and confidence, ensuring that each textual reference is reconciled to a single, queryable concept that supports fair benchmarking and faithful reproduction of setups.

**C. Implicit/Abstracted Entities.** Beyond what is explicitly named, we synthesize high-value abstractions that capture *what the paper claims, assumes, and finds*, which are indispensable for cross-paper reasoning. Using rhetorical-role tagging and discourse parsing, we aggregate sentences across sections to construct a formal *Problem Definition* ( $\mathcal{X}, \mathcal{Y}, C, \mathcal{A}$ ) specifying input/output spaces, constraints, and assumptions (e.g., independence/stationarity); codify *Motivations/Gaps* into a taxonomy (data

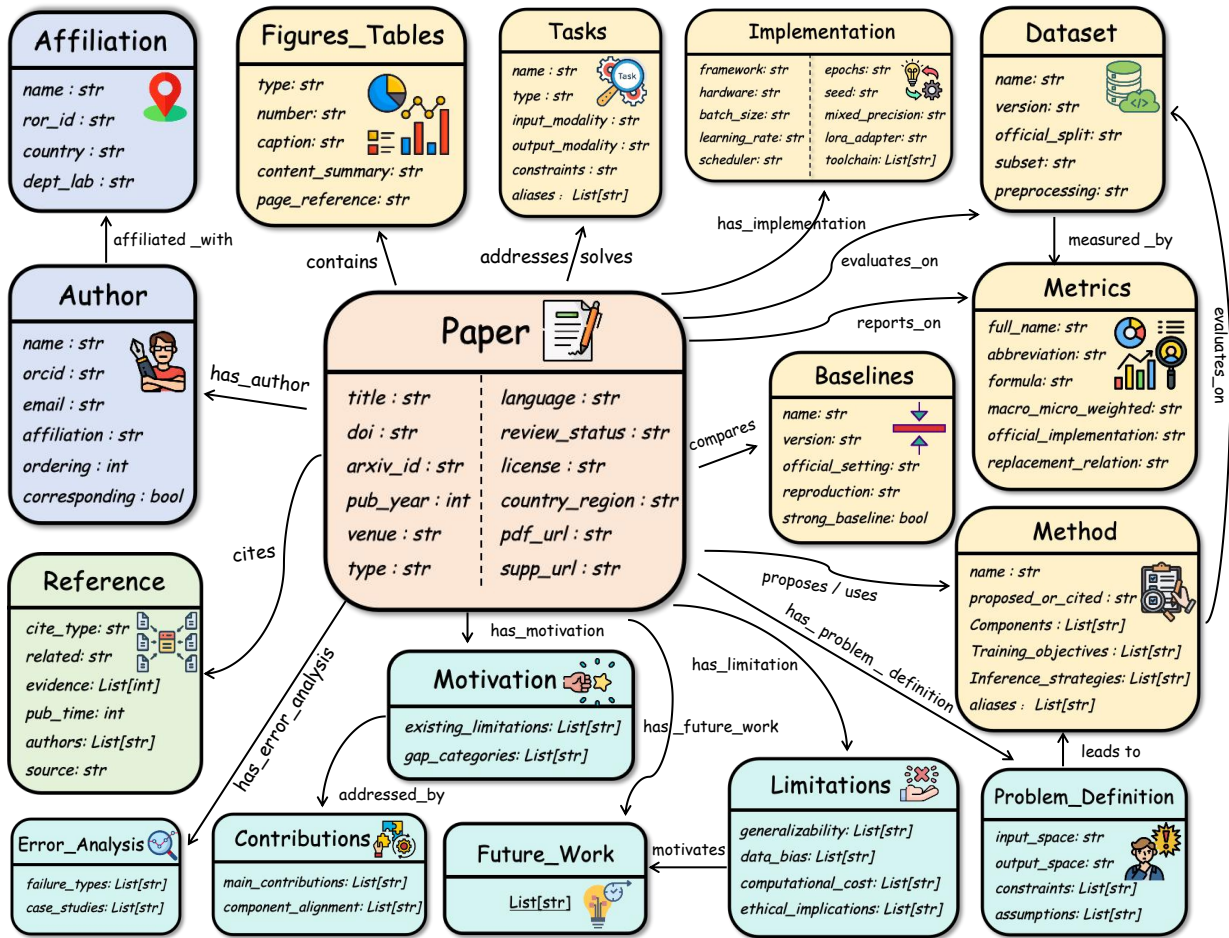


Figure 4 | Disaggregated Schema of our KG. This schema illustrates the structural decomposition of a multimodal scientific document into a unified, queryable knowledge graph. By explicitly modeling these entities and their interconnected relationships, the schema dismantles unstructured text to furnish AI agents with a rigorous reasoning infrastructure. For detailed examples, please refer to Appendix D.

efficiency, long-range dependence, tool-integration failure, etc.); align bulletized *Contributions* to concrete components so that each improvement is attributable; register *Hypotheses/Assumptions* with testability flags and scope; extract *Findings/Claims* with quantitative effect sizes and qualitative patterns (consistency, robustness, scaling behavior); record *Explanations/Mechanisms* (causal, mechanistic, or heuristic rationales) that account for observed results; and document *Limitations/Threats* (external validity, biases, compute cost, ethics), *Design Rationales*, *Future Work/Open Questions*, and *Error Analyses/Case Studies*. These abstracted nodes are evidence-linked and confidence-calibrated, merged across documents when semantically equivalent, and provide a structured infrastructure for causal-aware synthesis, systematic reviews, and meta-analyses.

**D. Citation Relationships.** We represent how the literature positions a focal work by encoding *who cites whom, how strongly, and to what argumentative effect*. Each *Citation* edge stores the cited paper’s identity (title, authors, year, DOI/venue), *Cite Type* (strong/weak, direct support vs. indirect mention, core reference flag), a one-sentence *Relation* (support/contrast/extend/background) with its argumentative role, fine-grained *Evidence* (section/paragraph indices, in-text spans, frequency),

temporal information (publication date and timeline ordering), and enriched *Author/Team* and *Source* signals (affiliations, collaborations, venue prestige). We compute a citation-strength score from frequency, rhetorical-zone coverage, lexical cues (e.g., “we adopt”, “we improve upon”), and proximity to key entities, and threshold it to label strong vs. weak citations; relation roles are predicted with cue-based classifiers and verified for high-impact cases via human-in-the-loop. The resulting citation layer, together with Modules A–C, yields a heterogeneous, provenance-rich knowledge graph that supports evidence-grounded retrieval, lineage tracing of datasets/metrics, identification of pivotal works, and causal mapping of how claims propagate and evolve across disciplines. For the detailed citation context classification schema, please refer to Appendix A.

**E. Knowledge Relations Between Entities.** Modules B and C already capture scientific knowledge, but at a coarse, paper-level granularity: B records explicitly mentioned objects and their attributes, while C aggregates motivations, mechanisms, and limitations as high-level nodes attached to each paper. Module E refines this into fine-grained triples between specific entities, so that knowledge previously encoded as paragraph-level abstraction becomes directly queryable. We organize the triples into two complementary families. Controlled relations require head and tail to already exist in Module B, preserving ontological discipline over the method, task, and dataset space; they include *BUILDS\_ON*, *USES\_COMPONENT*, *ALTERNATIVE\_TO*, *SOLVES*, *APPLIED\_TO*, and *TARGETS*. Open relations admit new concepts when a mechanism lacks a canonical name, spanning four semantic zones: causal (*CAUSES*, *ENABLES*, *INHIBITS*, *MODULATES*, *CORRELATED\_WITH*), internal composition (*USES\_TECHNIQUE*, *CONSISTS\_OF*, *IMPLEMENTS*, *COMBINES*, *REQUIRES*), methodological comparison (*DERIVED\_FROM*, *DIFFERS\_FROM*, *HAS\_LIMITATION*, *ADDRESSES\_PROBLEM*, *MOTIVATED\_BY*), and domain structure (*HAS\_PROPERTY*, *SUBSET\_OF*). By design, this layer admits only durable knowledge: numerical results, hyperparameters, and experimental setups are excluded, because they either already reside under Module B or vary across replications and would dilute the graph with ephemeral noise. Triples arrive through two reinforcing channels. Structural edges are materialized deterministically from Modules A and B, for instance *AFFILIATED\_WITH* built from author metadata or *USES\_COMPONENT* from declared submodules. Semantic edges are mined with section awareness, harvesting causal claims primarily from Introduction and Discussion, internal composition from Methods, comparative gaps from Related Work, and failure modes from Limitations, with alias reconciliation against Module B to prevent entity fragmentation. Each triple records  $\langle \text{head}, \text{head\_type}, \text{relation}, \text{tail}, \text{tail\_type} \rangle$  with a verbatim evidence span, calibrated confidence, and a source tag distinguishing semantic from structural provenance; semantically equivalent triples are merged across documents via canonicalization over entity embeddings. Together with Modules A through D, this relational layer refines coarse abstractions into a structure that can be traversed and reasoned over, turning the graph from a catalog of entities into a navigable reasoning surface that supports multihop causal tracing, architectural provenance, methodological lineage comparison, and cross-paper synthesis of limitations and design rationales that would otherwise remain buried in prose.

## 4.2. Dataset Construction via LLM-Guided Multi-Hop QA Generation.

Beyond constructing Scholar-KG, the same structured paper representation can be reused to synthesize evidence-grounded multi-hop QA data, which serves as an additional downstream artifact of the KG construction pipeline.

Given a corpus of academic papers  $\mathcal{P} = \{p_j\}_{j=1}^M$ , where each paper is represented as a structured JSON object containing metadata and full text, our objective is to automatically construct a high-quality multi-hop reasoning QA dataset  $\mathcal{D}$ . Each QA instance is designed to probe deep paper understanding and consists of a complex question requiring 3–5 explicit reasoning steps, an exact and unambiguous

answer that is a concrete term or method stated in the paper, an ordered chain of factual statements sufficient to derive the answer, explicit textual evidence from the source paper, and a structured entity–relation graph. To make the generation tractable within the model context window while preserving sufficient information, we first transform each paper  $p$  into a compact prompt representation

$$S(p) \triangleq \text{concat}(\text{metadata}, \text{abstract}, \text{content}[:L]),$$

where  $L$  is a fixed truncation threshold. This summary is embedded into a unified prompt  $\Pi(p)$  composed of a reusable schema-constrained template and task-specific instructions, ensuring that the model produces exactly five QA instances per paper with consistent structure and explicit evidence grounding.

**Structured Generation, Validation, and Quality Control.** We formulate QA construction as a conditional text-to-structure generation problem using a large language model  $\mathcal{M}_\theta$ , which maps the paper-specific prompt to a structured JSON output:

$$\hat{Y}(p) \sim \mathcal{M}_\theta(\Pi(p); \tau),$$

where  $\tau$  denotes the decoding temperature. The model is strictly instructed to output a valid JSON array of five objects, each containing a question, an exact answer, a multi-hop chain of key facts, source evidence excerpts, and an entity tree encoding entities and typed relations. To ensure reliability and suitability for benchmark construction, we apply a robust post-processing and validation pipeline that enforces structural correctness, non-emptiness of all fields, answer faithfulness to the paper text, logical sufficiency of the reasoning chain, and well-formedness of the entity graph. This combination of constrained prompting and deterministic validation yields a scalable and reproducible procedure for generating high-quality, evidence-grounded multi-hop QA data from scientific literature, while remaining agnostic to the underlying inference backend (API-based or locally hosted models).

### 4.3. General-KG: A Multi-View, Schema-Adaptive Extension to Arbitrary Documents

Our KG schema introduced above specialises to peer-reviewed scientific literature and commits to the five-module Module A through E decomposition. Many downstream deployments require the same infrastructure to run over heterogeneous corpora such as medical reports, legal filings, and financial disclosures, and require different graph granularities over the same document: lexical retrieval prefers compact binary triples, multi-hop reasoning prefers  $n$ -ary hyperedges that keep co-occurring arguments bundled, and event tracking prefers edges carrying explicit temporal qualifiers. General-KG addresses these requirements with a multi-view, schema-adaptive extension that reuses the OCR front-end, the semantic-anchor layer, and our model extraction backbone, while replacing the fixed schema with a family of pluggable views and a cold-start procedure that adapts to new verticals without weight updates.

**Multi-View Mode Family.** General-KG exposes the same document through six complementary views, each implemented as an independently registered mode that produces a uniform payload with typed nodes  $\mathcal{V}$ , hyperedges  $\mathcal{E}_n$ , evidence spans, and source-chunk provenance. Table 1 lists the modes and their target tasks. The modes are compositional rather than exclusive: a typical deployment activates several at once and lets the agent layer route per query. The set is open; registering a new mode requires a decorator in a new module directory, with no change to the shared pipeline.

Table 1 | The six graph views exposed by General-KG. All modes share a common output schema so that downstream retrieval and agent code remain mode-agnostic. Projection modes derive their output deterministically from the core artifact; upgrade modes issue one additional LLM pass per chunk on top of the core.

Mode	Graph form	Best-fit downstream task	LLM calls / chunk
binary	triple $(h, r, t)$	lexical retrieval, path queries	0 (projection)
nary	hyperedge, $k \geq 3$	multi-hop QA with bundled arguments	1 (upgrade)
temporal	edge + time qualifier	timeline reasoning, change tracking	1 (upgrade)
person	person-centric subgraph	biography, compliance, author graph	0 (projection)
event	event node + roles	narrative, FrameNet-style analysis	1 (upgrade)
diy	YAML-declared schema	medical, legal, financial verticals	1 (upgrade)

**Core-then-Modes Architecture.** Running  $M$  independent extraction pipelines would multiply LLM cost by  $M$  and would defeat the multi-view story on corpora of realistic size. We instead factor the extraction into a shared core stage and a family of mode stages. Given a document segmented into chunks  $\{c_i\}_{i=1}^n$ , the core stage produces a canonical typed entity set and a binary relation skeleton,

$$(\mathcal{V}_{\text{doc}}, \mathcal{E}_{\text{skel}}) = f_{\text{core}}(\{c_i\}_{i=1}^n), \quad (3)$$

using two LLM passes per chunk: the first extracts typed entities and merges them across chunks by case-insensitive canonical name, and the second is conditioned on the merged entity set and extracts strictly binary relations with evidence quotes, rejecting any triple whose head or tail falls outside  $\mathcal{V}_{\text{doc}}$ . Each mode then consumes  $(\mathcal{V}_{\text{doc}}, \mathcal{E}_{\text{skel}}, \{c_i\})$  and dispatches to one of two strategies. Projection modes (binary, person) derive their output deterministically by filtering and relabelling the skeleton, and cost zero additional LLM calls. Upgrade modes (nary, temporal, event, diy) issue one LLM pass per chunk that takes the skeleton as a structural anchor and lifts it into the target form, for example by merging co-occurring binary edges into hyperedges of arity  $k \geq 3$ , or by attaching time qualifiers drawn from  $\{\text{POINT\_TIME}, \text{START\_TIME}, \text{END\_TIME}, \text{BEFORE}, \text{AFTER}\}$ . Because the entity set is canonicalised once in the core, every upgrade pass operates on a strictly smaller hypothesis space than an end-to-end extractor would face, which both shortens the prompt and empirically reduces hallucinated participants. Letting  $n_{\text{up}}$  denote the number of activated upgrade modes and  $M$  the total number of activated modes, the per-document cost satisfies

$$C_{\text{ours}} = n \cdot (c_{\text{core}} + n_{\text{up}}) \leq C_{\text{naive}} = c_{\text{core}} \cdot n \cdot M, \quad (4)$$

with  $c_{\text{core}} = 2$  in our implementation. For a representative all-views configuration with  $n = 8$ ,  $n_{\text{up}} = 4$ , and  $M = 6$ , the factoring reduces LLM calls from 96 to 48, a fifty percent saving, while producing the full six-view output. A second structural benefit is that every view references the same node identifiers, so cross-view joins such as pivoting from a binary retrieval hit to the nary hyperedges that contain the same head entity reduce to identifier lookup rather than fuzzy string matching. This property is what later allows the CLI layer to treat different views as interchangeable retrieval sources.

The mode family above answers how a document is viewed; it does not answer what the extractor should look for in a vertical that our model has never seen. Hand-authoring a prompt for every vertical is slow, does not scale across customers, and loses ground as the corpus drifts. We therefore attach a weight-frozen self-improvement loop that distils a reusable skill library from a small seed of gold annotations. Given 10 to 20 hand-curated gold documents per vertical, the loop proceeds in four phases per gold document. In the rollout phase, the current extractor is sampled  $K$  times with non-zero decoding temperature to elicit genuine sampling variance, producing candidate edge sets  $\{R_k\}_{k=1}^K$ . In the classify phase, every gold edge  $e^*$  is scored against  $\{R_k\}$  under a matcher that

normalises the relation to `UPPER_SNAKE_CASE` and treats participants as a case-insensitive set, yielding the label

$$\text{label}(e^*) = \begin{cases} \text{STABLE} & \text{if } e^* \text{ matches for all } k \in [K], \\ \text{UNSTABLE} & \text{if } e^* \text{ matches for some but not all } k, \\ \text{MISS} & \text{otherwise.} \end{cases} \quad (5)$$

`STABLE` edges are already handled reliably and are skipped. `UNSTABLE` edges drive path induction, in which the LLM is given the evidence span of  $e^*$  and asked to verbalise a minimal trigger pattern that would have produced the edge on every rollout. `MISS` edges drive hindsight reasoning, in which the LLM is given both the gold edge and the extractor’s failing output, asked to diagnose why the edge was plausibly missed, and asked to propose a corrective pattern. Both paths yield candidate skills anchored by concrete evidence quotes, which we find essential for downstream retrievability. A deterministic controller then folds each candidate skill into the library under one of four actions (`ADD`, `MODIFY`, `MERGE`, `KEEP`), using Jaccard similarity over pattern tokens with a tunable threshold to decide overlap. At inference time, a lightweight retriever scores every skill against the document title and the first 2,000 characters of body text and prepends the top- $k$  skills (default  $k = 3$ ) to the core-extraction system prompt; when the library is empty or the activation flag is off, the retriever returns an empty context and the pipeline is byte-identical to the skill-free baseline, so the skill loop is a pure addition rather than a required path. Leaving our model weights untouched yields three properties that matter in deployment: cold-starting a new vertical requires no GPU run, cross-domain regression at the weight level is impossible by construction, and every skill is human-auditable and version-controlled, which is decisive in regulated domains where prompt provenance is a compliance concern rather than a nice-to-have.

**DIY Schema via YAML.** Some verticals require entity and relation types that fall outside the five built-in modes, for example `DRUG`, `ENZYME`, and `ADVERSE_EFFECT` for drug interaction analysis, or `PARTY`, `OBLIGATION`, `DEADLINE`, and `PENALTY` for contract review. Implementing a new extraction mode in Python for every such vertical couples schema evolution to code-deployment cycles, which is unacceptable in regulated domains. The `diy` mode therefore consumes a self-contained YAML template that declares `entity_types`, `relation_types`, `qualifiers`, and a few-shot example block; at runtime the mode parses the template, assembles a schema-conditioned prompt from the few-shot block, and dispatches one LLM call per chunk in the same shape as the other upgrade modes, which keeps the cost formula of Eq. 4 intact. The YAML template and the skill library compose cleanly: the template fixes the target ontology and supplies a small number of canonical examples sufficient to stand up a functional pipeline, and the skill library then accumulates domain-specific extraction patterns that operate within that ontology. The result is that the marginal cost of onboarding a new vertical becomes dominated by gold annotation time rather than by engineering time.

**Relation to our KG.** General-KG is a parallel track rather than a replacement. Our KG remains the canonical choice for academic corpora where the five-module schema is exactly the intended output and where citation structure and method lineage are first-class concerns. General-KG is the canonical choice for arbitrary documents where multi-view, schema-adaptive output is required and where the ontology itself evolves with the corpus. The two tracks share the OCR front-end, the semantic-anchor layer, and our model extraction backbone, and they converge at the CLI layer, which treats their outputs as interchangeable retrieval sources mediated by the tri-source adaptive fusion mechanism.

#### 4.4. Knowledge Organization and Storage

The extracted entities and relations are organized into a heterogeneous knowledge graph  $\mathcal{G} = (\mathcal{V}, \mathcal{E}, \mathcal{R})$ , where  $\mathcal{V}$  is the set of entity nodes,  $\mathcal{E}$  is the set of typed edges, and  $\mathcal{R}$  is the set of relation types. We adopt a graph database (e.g., Neo4j) for flexible schema management and efficient graph traversal queries.

**Indexing for Retrieval.** To support efficient retrieval in downstream applications, we construct multiple indices: (i) a text index over entity names and descriptions using BM25, (ii) a vector index over entity embeddings for semantic search, and (iii) a graph index for fast neighborhood queries. Each entity node stores provenance information linking back to source documents, enabling evidence-grounded responses.

**Versioning and Updates.** As new papers are added to the corpus, we incrementally update the knowledge graph by detecting new entities, merging duplicates, and updating citation counts. Entity linking ensures that mentions in new papers are connected to existing canonical entities, maintaining graph coherence over time.

#### 4.5. Theoretical Foundations

Our scientific KG of Section 4.1 and the General-KG mode family of Section 4.3 use the same entity identifier space. Each node has a stable entity identifier, while canonical names and aliases are stored as attributes rather than used as join keys. This subsection explains why that design is useful for retrieval. The statements below describe the candidate stage before final ranking or truncation, and assume that entity identifiers have been assigned correctly. Errors from extraction, entity linking, and ranking are evaluated empirically in Section 7. Proofs and constructive details are deferred to Appendix B.

We treat the extraction of a document  $D$  as a single payload  $\mathcal{P}_D = (\mathcal{V}, \mathcal{E}_h)$ , where  $\mathcal{V}$  is a finite set of typed nodes with globally unique identifiers and  $\mathcal{E}_h \subseteq \bigsqcup_{k \geq 2} \mathcal{V}^k$  is a set of typed hyperedges. Nodes and edges also carry evidence spans and chunk-level provenance, which we omit from the notation. A **view** is a deterministic map  $\Phi_v: \mathcal{P}_D \mapsto \mathcal{P}_v$  that filters edges, qualifiers, or types but does not rename nodes. In particular,  $\mathcal{V}_v = \mathcal{V}$  for every view  $v$ . Our scientific KG and the six modes of Table 1 are all views in this sense, and the *union view*  $\mathcal{P}_U \triangleq \bigsqcup_{v \in \mathcal{V}} \Phi_v(\mathcal{P}_D)$  keeps the same node identifiers.

**Definition 1** (ID-Respecting Retriever). *A candidate retriever  $\Phi_R$  is ID-respecting if it uses node identifiers as join keys and is monotone in the edge set, i.e.  $\mathcal{G}_1 \subseteq \mathcal{G}_2$  implies  $\Phi_R(\mathcal{G}_1, q) \subseteq \Phi_R(\mathcal{G}_2, q)$  before final ranking and truncation. BM25 over canonical names, dense retrieval over name embeddings, and graph traversal qualify when their candidate sets are joined by stable node identifiers.*

The first design choice is to key every view by a globally unique node identifier rather than by canonical name. Surface-form alignment, the natural alternative, has a worse asymptotic cost and exposes the system to false merges whenever distinct entities share the same string. The following proposition makes both observations precise.

**Proposition 1** (Identifier Preserving Joins). *Let  $\Phi_u, \Phi_v$  be two views and  $K \subseteq \mathcal{V}$  a node-key set. If both views preserve the same stable identifiers, the cross-view join  $\Phi_u(\mathcal{P}) \bowtie_{\mathcal{V}} \Phi_v(\mathcal{P})$  on  $K$  can be implemented as a hash join in  $O(|K|)$  time. If two views are produced by independent pipelines and have no shared identifiers, alignment must rely on surface form comparison. For unconstrained pairwise similarity without a blocking key or metric structure, the worst-case cost is  $\Omega(|\mathcal{V}_u| \cdot |\mathcal{V}_v|)$ . Let  $\sigma(v)$  denote the surface form of node  $v$ , and let  $H = \{v \in \mathcal{V} : |\sigma^{-1}(\sigma(v))| \geq 2\}$  be the homonym set. When  $H$  is nonempty,*

matchers that merge identical surface forms can introduce false merges:

$$\Pr_{v \sim H, w \sim \mathcal{V}} [w \neq v, \sigma(w) = \sigma(v)] = \frac{\sum_{v \in H} (|\sigma^{-1}(\sigma(v))| - 1)}{|H| \cdot |\mathcal{V}|}. \quad (6)$$

A single binary projection (subject–predicate–object) collapses any fact that involves three or more participants, for example a temporal qualifier or a multi-argument experimental condition. We next show that the union view never reaches fewer nodes than a single view, and reaches strictly more whenever the gold reasoning path traverses a hyperedge of arity at least three.

**Proposition 2** (Cross View Reachability). *Let  $R_h(\mathcal{G}, q) \subseteq \mathcal{V}$  be the set of nodes reachable in at most  $h$  hops from a query-anchored seed  $S(q)$  in  $\mathcal{G}$ , with each hyperedge of arity  $k \geq 2$  counting as one hop connecting all of its endpoints. Then for every query  $q$ :*

1. **Monotonicity.** *The union view contains every node reachable in any single view:  $R_h(\mathcal{P}_U, q) \supseteq R_h(\Phi_v(\mathcal{P}_D), q)$  for every  $v$ .*
2. **Strict gap.** *If a gold reasoning path uses a hyperedge of arity at least three, a binary projection may hide some endpoints of that edge. Let  $H_{\geq 3}^{(h)}(q)$  be the gold  $\geq 3$ -arity hyperedges that lie on a gold  $h$ -hop reasoning path. For each  $e \in H_{\geq 3}^{(h)}(q)$ , let  $B_e$  be the endpoints of  $e$  that are reachable from  $S(q)$  only through  $e$  and are not retained by the binary view. Then*

$$|R_h(\mathcal{P}_U, q) \setminus R_h(\Phi_b(\mathcal{P}_D), q)| \geq \left| \bigcup_{e \in H_{\geq 3}^{(h)}(q)} B_e \right|. \quad (7)$$

*In the common two-anchor case with disjoint hidden endpoint sets, the right-hand side equals  $\sum_{e \in H_{\geq 3}^{(h)}(q)} (|e| - 2)$ .*

*Recovering the hidden higher-arity structure from the binary view alone is hard in the worst case; Appendix B gives the reduction.*

The reachability gap above translates directly into a candidate-stage recall bound. The union view’s recall is at least the best single-view recall plus the fraction of gold answers that only the joined view exposes, which is exactly the quantity stress-tested in Section 7.

**Proposition 3** (Candidate Coverage). *Let  $\Phi_R$  be an ID-respecting candidate retriever. Let  $A_h^*(q) \subseteq \mathcal{V}$  be a nonempty gold  $h$ -hop answer set, and let  $\rho_h(\mathcal{G}, q) = |\Phi_R(\mathcal{G}, q) \cap A_h^*(q)| / |A_h^*(q)|$  be the candidate-stage recall. Define*

$$\Delta_h(q) = \frac{|A_h^*(q) \cap (\Phi_R(\mathcal{P}_U, q) \setminus \bigcup_v \Phi_R(\Phi_v(\mathcal{P}_D), q))|}{|A_h^*(q)|},$$

*the fraction of gold answers retrieved only after the views are joined. Then*

$$\rho_h(\mathcal{P}_U, q) \geq \max_v \rho_h(\Phi_v(\mathcal{P}_D), q) + \Delta_h(q), \quad (8)$$

*where  $\Delta_h(q) \geq 0$ . Proposition 2 gives one condition under which this term is positive: the gold path uses evidence that is visible in the union view but hidden by a single binary projection. Thus, adding an identifier-preserving view can expand the candidate evidence available before the final ranker selects its top results.*

Together, these propositions state a simple design principle. Stable identifiers make evidence from different views easy to join; multiple views expose evidence that a single binary projection may miss; and the joined candidate set can cover more gold evidence before ranking. The witness construction in Appendix B turns the strict gap term into a concrete stress test, and the queries used in Section 7 are constructed to exercise it.

## 5. LLM Layer: Reinforcement-Learned Information Extraction Backbone

The knowledge graph and scientific knowledge network described in Sections 4 provide the structural scaffolding for downstream retrieval and reasoning, but their practical utility is tightly coupled to the accuracy of the information extraction module that populates them. Noisy or incomplete entity and relation extraction propagates directly into retrieval errors and degraded agent decisions. Rather than rely on a general-purpose instruction model for this step, we train a compact, domain-specialised IE backbone via reinforcement learning with a rule-based reward. The resulting model starts from *Qwen3-4B-Instruct* and is optimised with GRPO. We describe the algorithm, the reward design, and the training data below.

### 5.1. Training Algorithm

At each step  $t$ , the current policy  $\pi_{\theta_{\text{old}}}$  samples a batch of  $B$  prompts from the training distribution  $\mathcal{D}$ . For every prompt  $q_b$ , we draw  $G$  independent rollouts  $\{o_{b,g}\}_{g=1}^G$  and score each rollout with a rule-based reward  $r_{b,g} = R(o_{b,g}, y_b^*, \tau_b)$ , where  $y_b^*$  is the ground-truth extraction and  $\tau_b$  is the per-sample task type (NER, RE, or STRUCT\_NER). The advantage is obtained by standardising rewards within each group:

$$\hat{A}_{b,g} = \frac{r_{b,g} - \mu_b}{\sigma_b + \epsilon}, \quad \mu_b = \frac{1}{G} \sum_g r_{b,g}, \quad \sigma_b^2 = \frac{1}{G} \sum_g (r_{b,g} - \mu_b)^2. \quad (9)$$

No value network is trained; the group means serve as the baseline. The policy is updated with the clipped PPO objective, regularised by a low-variance KL penalty to the frozen reference  $\pi_{\text{ref}} = \pi_{\theta_0}$  that is added as a loss term rather than folded into the reward:

$$\mathcal{L}_{\text{PG}}(\theta) = -\mathbb{E} \left[ \min \left( \rho_{b,g} \hat{A}_{b,g}, \text{clip}(\rho_{b,g}, 1 - \epsilon_{\text{clip}}, 1 + \epsilon_{\text{clip}}) \hat{A}_{b,g} \right) \right], \quad (10)$$

$$\mathcal{L}_{\text{KL}}(\theta) = \beta \cdot \widehat{\text{KL}}_{\text{IV}}(\pi_{\theta} \parallel \pi_{\text{ref}}), \quad (11)$$

$$\mathcal{L}(\theta) = \mathcal{L}_{\text{PG}}(\theta) + \mathcal{L}_{\text{KL}}(\theta), \quad (12)$$

where  $\rho_{b,g} = \pi_{\theta}(o_{b,g} | q_b) / \pi_{\theta_{\text{old}}}(o_{b,g} | q_b)$ . The full procedure is summarised in Algorithm 1.

### 5.2. Reward Function

Let  $\hat{y}$  denote the content parsed from the `<answer> . . . </answer>` span of a rollout  $o$ . We define a rule-based reward  $R(o, y^*, \tau) \in [0, 1]$  as the sum of three components:

$$R(o, y^*, \tau) = R_{\text{fmt}}(o) + R_{\text{json}}(o) + R_{\text{F1}}(o, y^*, \tau), \quad (13)$$

$$R_{\text{fmt}}(o) = 0.1 \cdot \mathbb{1}[\langle \text{think} \rangle \text{ present}] + 0.1 \cdot \mathbb{1}[\langle \text{answer} \rangle \text{ present}], \quad (14)$$

$$R_{\text{json}}(o) = 0.1 \cdot \mathbb{1}[\hat{y} \text{ parses as dict}] + 0.05 \cdot \mathbb{1}[\hat{y} \text{ is valid JSON but not dict}], \quad (15)$$

$$R_{\text{F1}}(o, y^*, \tau) = 0.7 \cdot \text{F1}_{\tau}(\hat{y}, y^*). \quad (16)$$

The format and JSON terms provide a dense shaping signal that is easy to optimise early in training, while the task-specific  $\text{F1}_{\tau}$  term carries the semantic signal. The F1 computation is dispatched by the per-sample task type  $\tau$ :

- $\tau = \text{NER}$ . Each value in  $\hat{y}$  and  $y^*$  is a list of entity strings keyed by entity type. Let  $E(y) = \{(t, \text{NORM}(e)) : t \in \text{keys}(y), e \in y[t]\}$ , where  $\text{NORM}$  lower-cases and trims the string. The score is the set-level F1 between  $E(\hat{y})$  and  $E(y^*)$ .
- $\tau = \text{RE}$ . Each value is a list of relation triples with `subject/object` fields. Let  $T(y) = \{(r, \text{NORM}(s), \text{NORM}(o))\}$ . The score is the set-level F1 between  $T(\hat{y})$  and  $T(y^*)$ .

---

**Algorithm 1** IE-GRPO Training
 

---

**Require:** base policy  $\pi_{\theta_0}$ , reference  $\pi_{\text{ref}} \leftarrow \pi_{\theta_0}$ , dataset  $\mathcal{D}$ , reward  $R$ , batch size  $B$ , group size  $G$ , PPO epochs  $K$ , clip  $\epsilon_{\text{clip}}$ , KL coeff.  $\beta$ , learning rate  $\eta$ .

- 1: Initialise  $\pi_{\theta} \leftarrow \pi_{\theta_0}$ ,  $\pi_{\text{old}} \leftarrow \pi_{\theta}$ .
- 2: **for**  $t = 1, \dots, T$  **do**
- 3:   Sample prompts  $\{q_b\}_{b=1}^B \sim \mathcal{D}$ .
- 4:   **for**  $b = 1, \dots, B$  **do** ▷ rollout phase
- 5:     Sample  $G$  responses  $\{o_{b,g}\}_{g=1}^G \sim \pi_{\text{old}}(\cdot | q_b)$ .
- 6:     Compute rewards  $r_{b,g} = R(o_{b,g}, \mathcal{Y}_b^*, \tau_b)$  for  $g = 1, \dots, G$ .
- 7:     Compute  $\hat{A}_{b,g}$  via group-relative standardisation.
- 8:   **end for**
- 9:   **for** epoch  $k = 1, \dots, K$  **do** ▷ update phase
- 10:    **for** each mini-batch  $\mathcal{M}$  of  $(q_b, o_{b,g})$  **do**
- 11:      $\rho_{b,g} \leftarrow \pi_{\theta}(o_{b,g} | q_b) / \pi_{\text{old}}(o_{b,g} | q_b)$ .
- 12:     Form  $\mathcal{L}_{\text{PG}}$  and  $\mathcal{L}_{\text{KL}}$  as in Eqs. (4)–(5).
- 13:      $\theta \leftarrow \theta - \eta \nabla_{\theta}(\mathcal{L}_{\text{PG}} + \mathcal{L}_{\text{KL}})$ .
- 14:    **end for**
- 15:   **end for**
- 16:    $\pi_{\text{old}} \leftarrow \pi_{\theta}$ .
- 17: **end for**

---

- $\tau = \text{STRUCT\_NER}$ . Used for long-form structured extraction with deeply nested schemas. For each top-level key  $k$  in  $y^*$ , we recursively flatten the subtree into a set of (path,  $\text{NORM}(\text{leaf})$ ) tuples, filtering placeholder leaves such as N/A, none, null, and compute a per-key  $F1_k$ . The final score is the macro-average over top-level keys,  $F1_{\text{STRUCT\_NER}} = \frac{1}{|\text{keys}(y^*)|} \sum_k F1_k$ , which prevents a single large branch from dominating the signal.

On top of this, set-level F1 follows the standard definition  $F1(A, B) = 2|A \cap B| / (|A| + |B|)$ , with both-empty sets treated as a perfect match.

## 6. CLI Layer: A Knowledge-Grounded Multi-Agent Research Toolkit

Sections 4 through 4.5 build the knowledge infrastructure: a multimodal hierarchical graph, a schema-adaptive extension to arbitrary documents (General-KG), an information-extraction backbone, and a formal account of how cross-view information linking expands candidate evidence. This section turns that infrastructure into a research agent. Our CLI departs from monolithic autonomous research agents along three axes. First, a tri-source retrieval mechanism combines web search, multimodal graph anchors, and cross-document network traversal under a shared evidence schema, using stable node identifiers when a source can be linked to the graph (Definition 1). Second, a small set of typed operators over the multimodal graph is exposed to the agent as deterministic primitives, so verifiable graph computation is separated from open-ended language reasoning. Third, a multi-role swarm execution layer composed of a coordinator, specialised workers, and an aggregator produces inspectable run artifacts rather than a single conversational answer.

The motivation is practical. A scientific task typically contains heterogeneous work that fails in different ways: retrieving recent papers, inspecting figures and tables, recovering method lineage, reading code, judging novelty, drafting a survey, and occasionally producing a prototype. Hiding all of this inside one chat loop makes the final answer hard to audit. Promoting it to a swarm of evidence-grounded roles makes intermediate objects (plans, evidence bundles, worker artifacts, manifests)

first-class. The same graph can therefore support paper survey, code understanding, idea grounding, idea generation, trend prediction, and idea-to-prototype workflows under a single execution model. For graph-linked evidence, the design realises the ID-respecting retriever of Definition 1, and so inherits the candidate coverage property of Proposition 3 before final ranking and truncation.

## 6.1. Tri-Source Knowledge Retrieval and Fusion

A fundamental limitation of existing autonomous research systems lies in their reliance on a single knowledge source. Web search gives broad coverage and recency but returns noisy, document-level results. Vector retrieval gives semantic recall but no structural reasoning. Pure graph traversal gives precision but no link to external recency. Our CLI uses a tri-source mechanism in which each source exposes a typed tool interface, and the agent decides, on a per-query basis, which sources to invoke and how to combine the evidence. Records that resolve to existing graph entities are keyed by the same stable node identifiers (Section 4.5), so their cross-source fusion is realised as a hash join rather than a fuzzy match. Web results that cannot yet be linked to a graph node are retained as document-level evidence and are not used in ID-based joins.

**Web Search ( $S_{\text{web}}$ ).** The web module accesses recent publications, preprints, and technical reports through academic search services such as arXiv, Semantic Scholar, and Google Scholar. Given a query  $q$ , it decomposes  $q$  into keyword combinations and scores each retrieved document  $d$  by

$$R_{\text{web}}(d, q) = \alpha_{\text{title}} \text{sim}(d_{\text{title}}, q) + \alpha_{\text{abs}} \text{sim}(d_{\text{abstract}}, q), \quad (17)$$

where  $\text{sim}(\cdot, \cdot)$  is a dense-embedding cosine similarity, and  $(\alpha_{\text{title}}, \alpha_{\text{abs}})$  are normalised weights with default (0.6, 0.4). The web module excels at recency: it surfaces work too new to have been ingested by the graph builder and provides the primary check for claims that fall outside the current graph snapshot.

**Multimodal Graph Retrieval ( $S_{\text{mmkg}}$ ).** The multimodal graph of Section 4 enables retrieval beyond text matching. For a query  $q$ , we identify relevant semantic anchors via a hybrid scheme that combines dense embedding similarity with lexical matching:

$$\mathcal{A}_{\text{relevant}}(q) = \{ a_j : \text{sim}(\mathbf{e}_q, \mathbf{e}_{a_j}) > \tau_{\text{anchor}} \vee \text{lex}(q, \text{desc}(a_j)) > \tau_{\text{lex}} \}, \quad (18)$$

where  $\mathbf{e}_q, \mathbf{e}_{a_j}$  are query and anchor embeddings and  $\text{lex}(\cdot, \cdot)$  is a token-overlap score over normalised labels and descriptions. Each retrieved anchor carries provenance  $\langle \text{doc\_id}, \text{page}, \text{bbox} \rangle$  for figure and table content, and  $\langle \text{file\_path}, \text{symbol}, \text{line\_span} \rangle$  for code anchors. The MMKG is the source through which figures, tables, and equations enter the agent loop as first-class evidence rather than caption-only proxies.

**Knowledge Network Traversal ( $S_{\text{kn}}$ ).** The scientific knowledge network of Section 4.1 supports cross-document reasoning over the heterogeneous graph of Modules A through E linked by typed relations such as `cites`, `proposes_method`, `uses_method`, `evaluates_on`, `compares_to`, and `reports_metric`. The traversal layer exposes deterministic graph primitives (Section 6.2) that the agent invokes as tools, providing precision and reproducibility while leaving open-ended reasoning to the LLM.

**Fusion.** The agent fuses the three sources into a typed bundle

$$\mathcal{K}_{\text{fused}}(q) = \text{TopK}_{e \in \mathcal{S}_{\text{web}}(q) \cup \mathcal{S}_{\text{mmkg}}(q) \cup \mathcal{S}_{\text{kn}}(q)} [\lambda_w s_w(e) + \lambda_m s_m(e) + \lambda_k s_k(e)], \quad (19)$$

where  $s_w, s_m, s_k$  are per-source normalised scores in  $[0, 1]$ , missing source scores are set to zero,  $(\lambda_w, \lambda_m, \lambda_k)$  are non-negative weights with default  $(0.30, 0.40, 0.30)$ , and the resulting set retains source labels, evidence type, reference id, and provenance fields so that the aggregator can later show which figure, paragraph, citation path, or code symbol supported each output. A lightweight intent classifier maps  $q$  to one of five categories, namely `recency`, `multimodal`, `lineage`, `comparative`, and `general`, and re-balances the weights accordingly: `recency` uses  $(0.70, 0.15, 0.15)$ ; `multimodal` uses  $(0.15, 0.70, 0.15)$ ; `lineage` and `comparative` use  $(0.20, 0.20, 0.60)$ ; `general` keeps the default. The classifier is a few-shot prompt over a frozen LLM and is called once per query, so the routing overhead is bounded by a single LLM call regardless of how many fan-out retrievals follow.

**Theoretical anchor.** For entries that are linked to graph nodes, Equation (19) is an instance of the ID-respecting retriever family of Definition 1. Every linked entry  $e$  is keyed by a stable node identifier from the shared vertex space  $\mathcal{V}$  of the universal payload, so cross-source joins are deterministic hash lookups (Proposition 1). Consequently, Proposition 3 implies that the fused candidate set for  $\mathcal{S}_{\text{web}} \cup \mathcal{S}_{\text{mmkg}} \cup \mathcal{S}_{\text{kn}}$  is at least as large in gold-answer coverage as the best linked single source, before final ranking and truncation. It becomes strictly larger when the joined sources retrieve additional gold candidates, i.e. when  $\Delta_h(q) > 0$ . Unlinked web records remain useful evidence, but they are outside this identifier-based guarantee until entity linking assigns them to  $\mathcal{V}$ .

## 6.2. Graph Operators and Multi-Agent Coordination

The agent does not operate on the graph as an unstructured text dump. Instead, it invokes a small set of typed operators that take a typed input and emit a typed output with explicit provenance, and a swarm execution layer composes these operators into research workflows. We describe the operator set first, then the swarm runtime that orchestrates them, and finally the tool surface through which both are exposed.

**(O1) Seed Resolution.** The deterministic primitive maps a candidate mention string to a canonical node set  $\mathcal{V}_{\text{seed}} \subseteq \mathcal{V}$  via case-insensitive label matching with degree-based disambiguation. Synonym expansion and contextual disambiguation are handled by the agent, which may issue multiple deterministic resolution calls before committing to a seed set.

**(O2) Citation Lineage Reconstruction.** Forward and backward traversal along `cites` edges, plus shortest-path queries weighted by lineage-bearing relations such as `BUILDS_ON`, `EXTENDS`, `DERIVES_FROM`, and `cites`, recovers method evolution chains across papers. The output is an ordered list  $\langle p_1, r_1, p_2, r_2, \dots, p_T \rangle$  of papers and the typed relations that connect them.

**(O3) Comparative Baseline Retrieval.** Given a dataset  $D$  and an optional metric  $M$ , returns all triples  $(P, m, v)$  such that  $P \xrightarrow{\text{evaluates\_on}} D$  and  $P \xrightarrow{\text{proposes\_method}} m$ . If  $M$  is provided, the query keeps only records with a matching `reports_metric` edge; otherwise  $v$  is returned when any reported value is available and marked missing when it is not. This realises the request “find all methods evaluated on  $D$  under  $M$ ” as a single graph query, without per-paper LLM inspection.

**(O4) Multimodal Anchor Retrieval.** Implements Eq. (18) and returns the relevant anchor set  $\mathcal{A}_{\text{relevant}}(q)$  together with the original payloads (cropped figure regions, serialised tables, LaTeX equations, code symbols) and bounding-box or line-span provenance.

**(O5) Gap Detection.** Surfaces structural indicators of under-explored regions: (i) orphan methods proposed but not reused, (ii) singleton datasets, (iii) papers disconnected from the main component, and (iv) sparse cells in the Method-Task projection  $(t, \mathcal{M}_t)$  where  $|\mathcal{M}_t| < \tau_{\text{cov}}$ . The output is a prioritised list of gap descriptors that the IdeaWorker can target.

**(O6) Idea Grounding and Novelty Judging.** Given a candidate idea  $I$ , it retrieves the top- $k$  most related methods  $\mathcal{R}_k(I)$  via O1 and O2, then asks an LLM judge  $\mathcal{J}_{\text{LLM}}$  to score methodological overlap on a structured rubric covering problem formulation, algorithmic mechanism, training strategy, and target domain:

$$\text{Novelty}(I) = \mathcal{J}_{\text{LLM}}(I | \mathcal{R}_k(I)) \in [0, 1]. \quad (20)$$

This formulation is intended to capture method-level novelty more directly than embedding cosine similarity, which can conflate surface form with methodological substance.

The split between deterministic operators and agent-mediated composition keeps each layer simple. Graph operations are efficient and verifiable, and the agent absorbs synonym handling, multi-step planning, and open-ended reasoning. Several capabilities therefore emerge from composition rather than from any single module: lexical seed resolution (O1) becomes semantic retrieval when the agent expands queries into synonyms; single-hop primitives (O2, O3) become multi-hop research workflows when the agent chains them with intermediate filtering; and structural retrieval (O5) becomes methodological novelty judgement when paired with an LLM rubric (O6).

**Swarm runtime.** We formalise a swarm run as follows. Given a graph  $G$ , a user task  $q$ , and an execution mode  $m \in \{\text{code-wiki}, \text{survey}, \text{idea-loop}, \text{all}\}$ , the coordinator emits a typed plan

$$\mathcal{P} = \text{Coord}(G, q, m) = \{j_i = (r_i, x_i, o_i, d_i)\}_{i=1}^n, \quad (21)$$

where  $r_i$  is the worker role,  $x_i$  is the payload,  $o_i$  is the output contract, and  $d_i$  is an optional dependency set. Each worker receives a compact evidence bundle drawn from  $\mathcal{K}_{\text{fused}}$  rather than the whole graph. The aggregator then writes

$$\mathcal{A} = \text{Agg}(\mathcal{P}, \{y_i\}_{i=1}^n, \{E_i\}_{i=1}^n), \quad (22)$$

where  $y_i$  is the worker output and  $E_i$  is the evidence used by that worker. The multi-role decomposition by itself is not novel, and we do not claim improved reasoning quality from the swarm structure. The three properties of Eq. (21) and Eq. (22) that matter for the rest of this report are concrete and narrow. First, the output contract  $o_i$  in  $\mathcal{P}$  is a typed schema rather than a free-form prompt, so worker outputs are checked against  $o_i$  before being accepted by the aggregator, and a failed contract becomes a routable signal rather than a silent textual error. Second, the run object  $\mathcal{A}$  is a manifest with on-disk artifacts, not conversation history, so a single worker can be rerun, a single evidence bundle replaced, or a single artifact audited without replaying the full session. Third, the dependency set  $d_i$  makes failure isolation computable: when a worker fails, the affected sub-tree is read off  $d_i$  rather than reconstructed from a chat trace, so recovery cost scales with the size of the dependent sub-graph rather than with the size of the whole plan. Worker-to-worker negotiation, debate, and majority voting are not part of the design, and the aggregator does not arbitrate disagreements between workers beyond accepting or rejecting outputs against  $o_i$ .

**Roles.** The Coordinator inspects the graph and the task and emits a plan. The CodeWikiWorker reads code communities and writes repository documentation. The SurveyWorker clusters paper nodes and writes topic sections. The IdeaWorker performs grounding (via O6), generation, critique, refinement, and novelty judging. The PrototypeWorker converts a selected idea into a method specification and a code scaffold. The Aggregator merges artifacts, writes the manifest, and surfaces failures rather than hiding them in a final summary. On worker failure, the Coordinator either retries the failing job with an enlarged evidence bundle for transient errors or replans the affected sub-tree for persistent errors. Failed jobs are recorded in  $\mathcal{A}$  verbatim so that downstream consumers can inspect them.

**Tool surface.** The deterministic graph primitives are exposed to the LLM through three concrete interfaces: a Python API for direct programmatic use, a unified command-line interface, and a Model Context Protocol (MCP) server that registers each primitive as a typed tool. We provide integrations for Claude Code via an `/graphanything` skill and for Nano-Claude-Code, while the MCP interface is designed to be provider-agnostic for agents that support typed tool calls. Table 2 summarises the complete tool surface, organised into four functional categories.

This split, with deterministic primitives below and agent-mediated composition above, keeps each layer simple: graph operations remain efficient and verifiable, while the agent layer absorbs synonym handling, multi-step planning, and open-ended reasoning. As a result, several capabilities of our framework emerge from composition rather than being implemented in any single module, which we treat as an explicit design choice rather than as an emergent property of prompt engineering.

### 6.3. Idea-to-Experiment Pipeline

Our CLI transforms research questions into method specifications and code prototypes through an iterative pipeline that couples knowledge retrieval, idea generation, novelty assessment, and code synthesis. Given a task description, the agent first retrieves background knowledge through the tri-source mechanism of Section 6.1. Retrieval proceeds from a broad survey stage to a focused deep-analysis stage, so that figures, tables, equations, and implementation details enter the loop together with prose.

**Iterative idea refinement.** The IdeaWorker generates diverse candidates and refines them through iterative critique:

$$I^{(t+1)} = G_{\text{LLM}}(I^{(t)}, C^{(t)}, \mathcal{K}_{\text{new}}), \quad (23)$$

where  $C^{(t)}$  is the structured critique at iteration  $t$  and  $\mathcal{K}_{\text{new}}$  is the freshly retrieved evidence. Initial iterations sample with high diversity; later iterations emphasise specificity and feasibility by incorporating targeted feedback from  $C^{(t)}$  and from new evidence retrieved in response to gaps surfaced at iteration  $t$ . Each candidate is assessed along four dimensions: coherence, credibility, feasibility, and novelty (Eq. 20). Novelty is grounded against the knowledge network rather than judged from the idea text alone, which helps steer the loop toward ideas that are specific, feasible, and easier to audit against prior work.

**From idea to method specification and code.** A promising idea is translated by the PrototypeWorker into a structured method specification covering problem formulation, algorithm design, and training strategy. The specification is iteratively refined for clarity and completeness against the same novelty rubric. The methodology is then converted into code, using existing repositories retrieved through the paper-to-code bridge of Section 4.1 as scaffolding. For complex methods, the system

Table 2 | Tool catalogue exposed by the CLI runtime. Each command is also available as a Python function and as an MCP tool.

Command	Function
<i>Ingestion</i>	
<code>graphanything ingest-kg merged_*.json</code>	Convert structured paper extraction JSON into a paper graph.
<code>graphanything add &lt;url&gt;</code>	Ingest a paper or code repository from a URL.
<i>Paper-level query (core primitives)</i>	
<code>graphanything find-paper "&lt;keyword&gt;"</code>	Search Paper nodes by keyword, DOI, arXiv ID, or author.
<code>graphanything paper-details "&lt;ref&gt;"</code>	Return a structured card: methods, datasets, contributions, citations.
<code>graphanything citations-of "&lt;ref&gt;"</code>	List papers cited by the given paper (outgoing).
<code>graphanything citations-to "&lt;ref&gt;"</code>	List papers that cite the given paper (incoming).
<code>graphanything lineage "&lt;A&gt;" "&lt;B&gt;"</code>	Shortest research-evolution path between two concepts.
<code>graphanything baselines "&lt;dataset&gt;"</code>	Methods evaluated on a dataset, optionally under a metric.
<code>graphanything tri-search "&lt;q&gt;"</code>	Route a query over web, multimodal anchors, and the knowledge network.
<i>Academic-metric analysis</i>	
<code>graphanything influential-methods</code>	Rank methods by structural influence in the graph.
<code>graphanything bridging-papers</code>	Identify papers that bridge distinct research communities.
<code>graphanything lineage-depth</code>	Compute the longest extension chain rooted at each method.
<i>Graph evolution</i>	
<code>graphanything evolve absorb</code>	Fold answered questions back into the graph as Question nodes.
<code>graphanything evolve compress</code>	Surface near-duplicate nodes as merge candidates.
<code>graphanything evolve gaps</code>	Detect orphan methods, singleton datasets, missing citations, detached papers.

decomposes the design into modular components and validates them incrementally,

$$\mathcal{M} = \{m_1, \dots, m_k\} \implies \mathcal{C} = \{C_1, \dots, C_k\}, \quad (24)$$

with errors resolved through an exception-guided debugging loop. The `PrototypeWorker` emits a prototype repository together with a smoke test that exercises the main entry point. Full reproduction of reported numerical results is not in scope of the smoke test and is treated as a downstream evaluation step rather than as a closed-loop signal at idea time. Accepted ideas, generated specifications, and prototypes are written back into the graph as `Hypothesis`, `MethodSpec`, and `Implementation` nodes through the explicit `graphanything evolve` command, so the graph records both literature and agent activity, but the gating decision is taken by the user rather than by the agent itself.

Table 3 | Representative downstream tasks supported by our CLI.

Task	Active workers	Output artifact
Idea grounding and evaluation	Coordinator, IdeaWorker, SurveyWorker	Claims, evidence paragraphs, similar / different points, novelty risks.
Idea generation	IdeaWorker, SurveyWorker, Aggregator	Candidate ideas with novelty, significance, risks, and key evidence.
Research trend prediction	SurveyWorker, IdeaWorker, Aggregator	Stage summaries, unresolved bottlenecks, future directions.
Paper-code bridge analysis	CodeWikiWorker, SurveyWorker, Aggregator	Mapping between method descriptions and implementation symbols.
Swarm execution audit	Coordinator, all selected workers, Aggregator	Plan, worker status, artifact paths, evidence ids, error messages.

### 6.4. Downstream Tasks and Examples

The system is best understood through downstream tasks. Each example below is rendered as an output card produced by a CLI run and saved by the aggregator. The structured field labels reflect the actual artifact schema rather than free prose, and the examples are intended as illustrative outputs rather than as benchmark numbers; quantitative comparisons are reported in Section 7.

#### Example: Idea Grounding and Evaluation

**Task:** Decide whether a target idea has genuine novelty after grounding it in related work.

**Target idea:** Evidence-Certified Scientific Idea Generation with a Coordinator-Worker-Aggregator Swarm.

**Target claim from the idea:** A research agent should not only output a new idea; it should also separate supported claims, new combinations, feasibility risks, and implementation anchors, so that novelty can be audited.

**Retrieved evidence:** Knowledge-graph-based scientific search retrieves papers and paragraphs for an idea, then compares the target claim with prior evidence across motivation, method, and experimental design.

**Matching aspect:** Knowledge-grounded idea evaluation.

**Similar point:** Both the target idea and the evidence treat idea evaluation as a grounding problem rather than as a pure language-model judgment, and both require retrieved evidence before judging novelty.

**Different point:** The evidence focuses on paper-and-paragraph grounding; the target idea adds a swarm execution layer, code anchors, manifest records, and separate worker roles for grounding, critique, and aggregation.

**Evaluation result:** The idea is not novel if stated only as retrieve-then-judge. Its stronger novelty comes from combining multimodal paper anchors, code-graph bridges, and an auditable swarm manifest into one research workflow.

#### Example: Idea Generation

**Command:** `graphanything swarm run -mode all -task "evaluate evidence-certified idea generation"`.

**Coordinator plan:** Launch one survey worker for the topic cluster, two code-wiki workers for implementation communities, and one idea worker for generation, critique, and novelty judging.

**Worker outputs:** The survey worker writes a topic section with citation lineage; the code workers write module notes and identify implementation anchors; the idea worker writes three candidate ideas and a

novelty comparison.

**Aggregator output:** A manifest with job ids, status, artifact paths, evidence ids, and failure messages, plus a readable report summarising the survey, implementation map, idea cards, and novelty risks.

**Audit value:** The user can rerun only the failed worker, replace one evidence bundle, or inspect the exact graph nodes that supported an idea, without re-issuing the entire prompt.

## 7. Experiments

This section evaluates Agents-K1 along four axes that collectively cover its three components and the empirical claim attached to its theoretical foundation. We first characterise the corpus that Agents-K1 is built on, reporting domain coverage across six scientific disciplines (Section 7.1) and the LLM-as-Judge evaluation protocol used throughout (Section 7.2). We then quantify our model extraction quality through the cross-domain breakdown of Section 7.3 and the head-to-head comparison against open-source extraction models at multiple parameter scales in Section 7.6. We turn next to the agent layer: Section 7.4 validates our CLI on knowledge-grounded scientific question answering, including geoscience research questions and the FRONTIERSCIENCE-RESEARCH benchmark, and Section 7.5 measures the same agent against nine graph-augmented retrieval baselines on HotpotQA, 2WikiMultiHopQA, and MuSiQue.

### 7.1. Domain Distribution and Coverage

To evaluate the scalability and domain adaptability of our framework, we constructed a large-scale heterogeneous scientific knowledge repository that ensures comprehensive coverage of major scientific disciplines. As illustrated in Figure 5, the dataset spans a diverse range of fields, predominantly encompassing Physics, Chemistry, Computer Science, Earth Science, Materials Science, Biology, and others, complemented by a significant collection of interdisciplinary literature. This broad domain distribution is critical for verifying the model’s robustness, ensuring it can effectively handle the varied terminologies, reasoning patterns, and data modalities inherent to different scientific contexts.

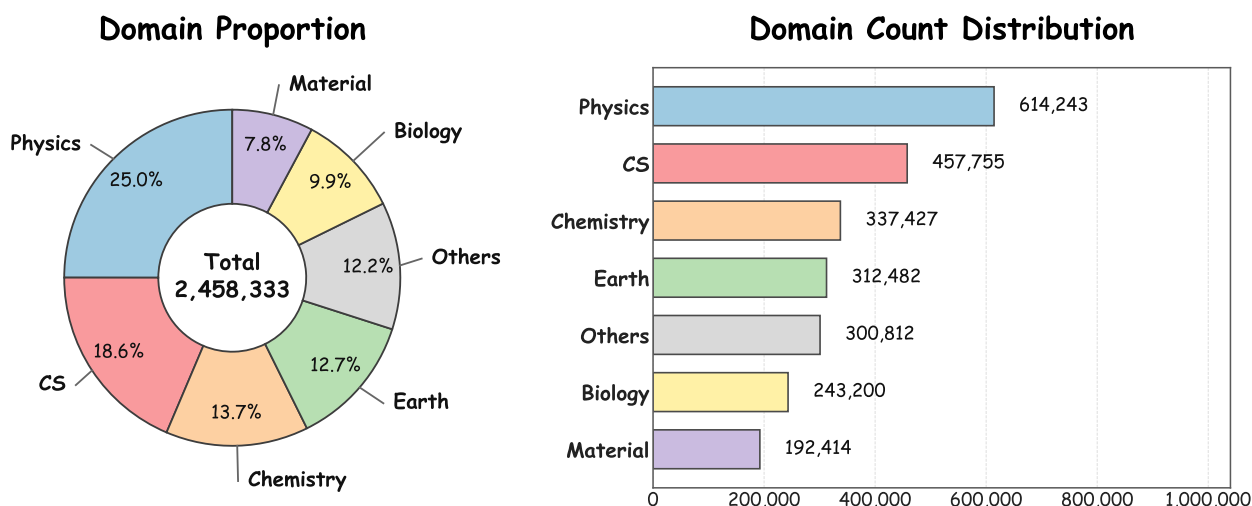


Figure 5 | Domain Proportion and Count Distribution, where CS represents computer science.

## 7.2. Evaluation Metrics

To comprehensively assess the quality of the constructed knowledge graph, we employ a rigorous **LLM-as-a-Judge** evaluation protocol. Unlike traditional exact-matching metrics, our framework utilizes a state-of-the-art large language model (DeepSeek-V3 [43]) acting as an “Expert Scientific Editor” to evaluate the extraction results based on semantic correctness and scientific essence.

### 7.2.1. Metric Formulations

We quantify performance using three standard metrics: **Precision** ( $P$ ), **Recall** ( $R$ ), and the **F1-score** ( $F1$ ). Let  $N_{ext}$  denote the total number of items extracted by the model. Through the LLM evaluation process, we identify  $N_{err}$  as the count of incorrect extractions (hallucinations or factual errors) and  $N_{miss}$  as the count of critical information omitted from the source text.

Accordingly, the number of correctly extracted items (True Positives) is defined as  $N_{correct} = N_{ext} - N_{err}$ . The estimated ground truth size is derived as the sum of correct items and missed items. The metrics are formulated as follows:

$$P = \frac{N_{ext} - N_{err}}{N_{ext}}, \quad R = \frac{N_{ext} - N_{err}}{(N_{ext} - N_{err}) + N_{miss}}, \quad F1 = \frac{2 \cdot P \cdot R}{P + R} \quad (25)$$

- **Precision** ( $P$ ): Reflects the *trustworthiness* of the system by penalizing hallucinations and factual contradictions.
- **Recall** ( $R$ ): Reflects the *completeness* of the system by penalizing the omission of core scientific concepts.
- **F1-score**: Serves as the harmonic mean to provide a holistic performance index.

### 7.2.2. Semantic-Aware Evaluation Criteria

To address the inherent complexity and heterogeneity of scientific literature, we developed a multi-dimensional evaluation protocol that transcends rigid keyword matching. Our framework distinguishes between *pedantic precision* (required for metadata) and *semantic understanding* (required for abstract concepts). As illustrated below, the evaluation is structured into four distinct modules, each governed by a specific judicial logic tailored to the nature of the information being extracted:

#### Module A: Meta/Factual Entities (Strict Verification)

This module evaluates the precision of objective metadata extraction (e.g., Authors, DOI, Affiliations). The evaluation follows a “**Zero-Tolerance for Hallucination**” policy:

- **Fine-Grained Verification**: The judge validates every single author name and institutional affiliation individually.
- **Fact vs. Inference**: Information is marked as *Incorrect* if it contains factual errors (e.g., wrong publication year). However, valid logical inferences (e.g., deriving the venue ‘arXiv’ from a specific DOI pattern) are accepted as correct.

### Module B: Textually Mentioned Entities (Semantic Tolerance)

This module assesses explicit entities such as Tasks, Methods, and Datasets. We adopt a “**Lenient on Format, Strict on Facts**” policy to handle terminological diversity:

- **Synonym Recognition:** Linguistic variations and abbreviations are deemed correct. For instance, extracting “ConvNet” when the text says “Convolutional Neural Network” is a valid match.
- **Core-Focus Recall:** The evaluation penalizes the omission of *primary* methods or *main* datasets. Missing trivial details (e.g., auxiliary hyperparameters like learning rates or generic terms like “computer”) does not negatively impact the Recall score.

### Module C: Implicit/Abstracted Entities (Abstractive Equivalence)

This module tests the system’s ability to synthesize high-level knowledge (Contributions, Findings, Limitations). The evaluation prioritizes **semantic essence over specific wording**:

- **Summarization Acceptance:** High-level summaries are accepted. If the text details specific numerical gains (e.g., “accuracy +5%”), an extraction stating “Performance Improvement” is considered correct.
- **Centrality-Based Assessment:** The system is penalized only if the *central scientific contribution* or the *main conclusion* is completely absent. Partial omissions of minor findings are tolerated.

### Module D: Citation Relationships (Hallucination Check)

This module evaluates the fidelity of the constructed citation network, ensuring the academic lineage is accurately preserved:

- **Existence Verification:** The judge strictly penalizes *hallucinated references*—citations generated by the model that do not exist in the source text’s bibliography.
- **Intent Consistency:** The inferred citation intent (e.g., whether a paper is cited as a baseline to *Contrast* or as a foundation to *Support*) must logically align with the context provided in the source text.

### Module E: Knowledge Relations Between Entities (Durable & Fine-Grained Triples)

This module extracts fine-grained relational triples to build a reasoning graph, enforcing a “**Durable Knowledge Only**” policy:

- **Noise Filtration:** Extracts must encode reusable scientific knowledge (e.g., causal claims, mechanisms). Ephemeral details like numerical results or hyperparameters are strictly penalized.
- **Strict Grounding:** *Controlled relations* must strictly align with entities in Module B. *Open relations* allow new concepts but require precise verbatim evidence from the text.

## 7.3. Cross-Domain Performance Analysis

Table 4 presents the comprehensive evaluation results across six distinct scientific domains. The framework demonstrates robust generalization capabilities, with the Average F1-score (AVG F1) consistently ranging from 79.07% to 87.11%. This stability confirms that our semantic-anchored architecture effectively adapts to the varied terminologies and reasoning patterns inherent to different

Table 4 | **Performance Comparison across Different Domains.** Note that the reported Precision (P), Recall (R), and F1 values represent the document-level macro-averages calculated over 100 distinct papers per domain and module.

Module	Metric	cs	chem	bio	earth	physics	material
Module A	P	85.16	90.17	90.29	90.07	91.53	94.38
	R	87.81	81.54	77.77	84.24	74.48	80.94
	F1	<b>85.12</b>	<b>84.72</b>	<b>82.65</b>	<b>85.88</b>	<b>81.24</b>	<b>86.52</b>
Module B	P	91.03	89.86	95.40	91.55	78.90	91.80
	R	82.00	74.14	80.18	76.82	68.36	79.31
	F1	<b>85.78</b>	<b>80.16</b>	<b>86.59</b>	<b>82.78</b>	<b>72.82</b>	<b>83.31</b>
Module C	P	94.05	96.06	90.71	97.25	96.76	97.50
	R	90.23	93.51	84.92	92.02	86.94	88.94
	F1	<b>91.84</b>	<b>94.59</b>	<b>87.22</b>	<b>94.33</b>	<b>90.90</b>	<b>92.55</b>
Module D	P	89.77	91.34	89.50	96.03	89.18	87.17
	R	79.44	83.74	84.16	85.33	75.04	79.06
	F1	<b>83.48</b>	<b>87.04</b>	<b>85.99</b>	<b>89.74</b>	<b>79.85</b>	<b>82.39</b>
Module E	P	93.07	81.48	80.00	87.53	76.17	77.37
	R	86.69	72.82	71.79	76.39	68.02	70.58
	F1	<b>89.33</b>	<b>75.64</b>	<b>74.23</b>	<b>80.39</b>	<b>70.54</b>	<b>72.67</b>
<b>AVG</b>	F1	<b>87.11</b>	<b>84.43</b>	<b>83.34</b>	<b>86.62</b>	<b>79.07</b>	<b>83.49</b>

disciplines.

**Domain-Specific Nuances** The performance variations reveal the unique characteristics of each scientific field:

- **Computer Science & Earth Science (Highest Consistency):** These domains achieved the top aggregate performances, with AVG F1 scores of 87.11% and 86.62%, respectively. The high scores in Module D (Citations) for Earth Science (89.74%) and the balanced results for Computer Science across all modules suggest that these fields follow highly standardized structural norms, facilitating precise information extraction.
- **Chemistry & Material Science (Deep Understanding):** Both fields exhibited remarkable performance in Module C (Implicit Entities), with Chemistry reaching an F1 of 94.59% and Material Science achieving 92.55%. This indicates the model’s superior capability to abstract complex reaction mechanisms and experimental properties into high-level conceptual findings.
- **Physics & Biology (Terminological Challenges):** While Precision remains high across most modules, these domains show a noticeable dip in Recall for explicit entities (e.g., Physics Module B Recall at 68.36%). This is attributed to the extreme diversity of non-standardized nomenclature and abbreviations prevalent in these disciplines, which poses a challenge for explicit entity matching.

**Module-Level Capabilities** Beyond domain differences, the module-wise breakdown highlights specific system strengths and sensitivities. Module C (Implicit Entities) emerges as the most robust component across the board, providing empirical evidence that the framework successfully transcends shallow pattern matching to capture the “scientific essence.” Module D (Citation Relationships)

also consistently yields reliable scores, confirming the system’s fidelity in reconstructing academic lineages. Conversely, the newly introduced Module E (Knowledge Relations) shows the highest variance across fields (ranging from an F1 of 70.54% in Physics to 89.33% in CS), demonstrating that fine-grained structural alignment is highly sensitive to the explicit reporting habits of specific scientific communities.

#### 7.4. Performance Comparison on Knowledgeable and Research Questions

**Efficiency for Geoscience Research.** In this section, we validate the effectiveness of the proposed scholarly knowledge graph framework in a geoscience-specific setting by performing a targeted schema adaptation. Building upon a general paper-citation graph backbone, we extend the schema with domain-specific entity and relation types to better capture key characteristics of geoscience research, namely, complex study objects, a multi-layered conceptual system, and strong dependence on spatiotemporal context. Concretely, we introduce and explicitly model several core concept nodes, including Region, Domain Terms, Geoscience Variables (e.g., carbon flux and seismic wave velocity), Geoscience Tasks (e.g., climate prediction and remote-sensing inversion), and Geoscience Formulae and Methods. These domain-specific entities are identified and extracted by a large language model through atomic-sentence-level parsing of paper content, and are then semantically linked to their corresponding paper nodes in the graph. This layered design preserves the universal citation structure while making the logical relationships among geoscience entities explicit, thereby providing structured support for scientific retrieval and reasoning.

Building on this schema extension, we construct a geoscience knowledge graph using Agents-K1 under a review-centric seeding with a citation-based expansion principle. We select 114 surveys/reviews from top-tier venues (AGU family journals, Reviews of Geophysics) published since 2025 as seed documents; their reference lists, after bibliographic normalization and deduplication, yield a citation corpus of 7,219 unique papers. Applying our information extraction pipeline to this corpus produces a heterogeneous graph with 602,132 nodes and 609,812 edges, mirroring how researchers in practice start from surveys and trace citation chains back to primary studies. The same review narratives further serve as expert-level references for evaluation, from which we derive two question categories: Knowledgeable Questions, targeting objective components such as variable definitions and formula applicability, and Research Questions, targeting field-level synthesis, competing viewpoints, and open problems. To prioritize multi-step reasoning, we retain questions whose answers require tracing citation links to source papers and integrating evidence across multiple atomic sentences; each test instance comprises a question, an answer, and a reasoning trace.

To quantify the benefit of Agents-K1, we conduct a controlled comparison between a standard large language model baseline and a graph-augmented retrieval generation model based on GraphRAG. The baseline relies on an LLM. In contrast, the GraphRAG-based model performs structured navigation and evidence retrieval over the geoscience knowledge graph before generation. It follows citation edges to identify relevant papers and their associated atomic-sentence evidence, and then conditions the final response on the retrieved evidence. Given the complexity of scientific reasoning, we adopt an LLM-as-a-judge protocol for automated evaluation. We use GPT-5.2 as the judge model and treat the review text as the reference ground truth (GT). For each output, the judge assigns a binary score (1/0) jointly over the reasoning trace and the final answer. The rubric evaluates, first, the validity of the reasoning process, namely, whether the model follows a coherent logical chain and integrates supporting evidence, and second, the correctness of the answer, namely, whether the conclusion is consistent with the expert statements in the review. This protocol evaluates not only outcome accuracy but also the traceability and rigor of the underlying reasoning.

Table 5 reports the performance of different models on knowledgeable questions and research questions,

Table 5 | Performance comparison on knowledgeable and research questions.

Model	Knowledgeable Questions		Research Questions	
	Rationale (%)	Answer (%)	Rationale (%)	Answer (%)
GPT-5.2	54.2	68.0	41.8	58.8
Gemini-3	58.3	71.2	52.3	61.0
GPT-5.2 w/ Agents-K1	65.8	75.0	66.3	69.7
Gemini-3 w/ Agents-K1	<b>67.5</b>	<b>77.9</b>	<b>69.5</b>	<b>71.5</b>

evaluated in terms of rationale accuracy and answer accuracy. Experimental results show that incorporating the graph substantially improves performance on multi-hop reasoning QA in geoscience. Overall, the GraphRAG-based model achieves higher accuracy than the baseline LLM. The gain is more pronounced on Research QA. This category requires synthesizing evidence across multiple papers, for example when summarizing methodological limitations or comparing findings across studies. The citation structure in the graph makes such scholarly dependencies and contrasts explicit, which provides a stable structural prior for retrieval and reasoning. Qualitative inspection further indicates that, for questions requiring precise evidential support, such as those about model limitations, the baseline tends to produce generic statements without attributable sources, whereas Agents-K1 more reliably traces citation links to the originating papers and retrieves atomic sentences labeled as limitations, leading to answers that are more specific and easier to verify. While a small number of failures remain, primarily due to incomplete extraction coverage or evidence loss over long reasoning chains, the results support the conclusion that combining citation-network structure with fine-grained information extraction improves both the reliability and interpretability of complex scholarly QA in a domain-specific setting.

**Efficiency for Scientific Research.** We further validate Agents-K1 in the broader scientific research domain using the FRONTIERSCIENCE-RESEARCH [12] benchmark. This benchmark consists of research-oriented questions from three core scientific disciplines: physics, chemistry, and biology. Unlike standard factual QA tasks, these questions require models to reason over specialized scientific concepts, experimental conditions, methodological assumptions, and field-level research findings. Each question is evaluated by a rubric-based scoring protocol, where credit is assigned according to whether the response correctly recovers the key scientific claims, supporting evidence, and reasoning steps expected by the benchmark. The benchmark is therefore substantially more challenging than conventional knowledge recall tasks: a model must not only identify relevant scientific knowledge, but also integrate it into a coherent research-level explanation. The low performance of pure reasoning baselines further confirms the difficulty of this setting, making it a suitable testbed for evaluating whether external scholarly knowledge can improve complex scientific reasoning.

To construct the external knowledge source for this benchmark, we build a task-specific scientific sub-knowledge graph guided by the keywords and topics of the benchmark questions. For each question, we search for relevant scholarly literature and collect documents that provide direct or indirect evidence for the corresponding scientific problem. Each paper is represented as a document node in the sub-knowledge graph, with structured attributes including title, abstract, content, source, and disciplinary label. We further organize the graph with question nodes, paper nodes, evidence nodes, and concept nodes by Agents-K1. Question nodes are linked to papers through retrieval edges, papers are connected to evidence nodes through content extraction edges, and evidence nodes are associated with scientific concepts or claims through semantic matching edges. This construction does not rely on a manually designed full-domain ontology; instead, it creates a lightweight but structured scientific knowledge graph centered on the benchmark questions. During inference, Agents-K1 first retrieves relevant paper and evidence nodes from the sub-knowledge graph, prioritizes evidence

Table 6 | Performance comparison on the FRONTIERSCIENCE-RESEARCH benchmark.

Model	Physics (%)	Chemistry (%)	Biology (%)	Overall (%)
Gemini-3	0.0	18.8	5.0	7.9
GPT-5.2	9.0	33.7	32.8	25.2
Gemini-3 w/ Agents-K1	13.8	31.3	28.8	24.6
GPT-5.2 w/ Agents-K1	<b>46.7</b>	<b>36.7</b>	<b>35.0</b>	<b>39.4</b>

according to its relevance and reliability, and then conditions the model’s final reasoning on the retrieved scholarly context.

Table 6 reports the performance of different models on the FRONTIERSCIENCE-RESEARCH benchmark. Compared with pure reasoning, Agents-K1 brings consistent overall improvements across both model families. For Gemini-3, the overall score increases from 7.9% to 24.6%, with substantial gains in all three disciplines. In particular, the biology score improves from 5.0% to 28.8%, indicating that the retrieved scientific evidence helps the model recover domain-specific biological knowledge that is difficult to infer from parametric knowledge alone. For GPT-5.2, Agents-K1 improves the overall score from 25.2% to 39.4%, mainly driven by a large gain in physics, where the score rises from 9.0% to 46.7%. These results show that incorporating an external scientific knowledge graph can improve research-level reasoning by grounding model outputs in relevant scholarly evidence. Overall, the experiment demonstrates that Agents-K1 is not limited to geoscience-specific reasoning, but can also generalize to broader scientific research problems where accurate answers require retrieving, organizing, and integrating evidence from specialized literature.

## 7.5. Performance on open source benchmarks

To further verify the universality of our proposed framework beyond domain-specific scientific literature, we conducted extensive evaluations on standard open-source multi-hop reasoning benchmarks.

### 7.5.1. Datasets and Evaluation Metrics

We utilized three widely adopted datasets designed to test multi-hop reasoning and retrieval capabilities: HotpotQA [13], 2WikiMultiHopQA [14], and MuSiQue [15]. HotpotQA and 2WikiMultiHopQA require reasoning over multiple supporting documents and entity relations, while MuSiQue offers a higher level of difficulty by minimizing shortcuts in reasoning chains. To comprehensively assess performance, we employ two metrics: Containment Accuracy (Contain-Acc.), which measures whether the exact answer string is present within the generated response to assess retrieval precision, and GPT-Judge Accuracy (GPT-Acc.), which utilizes a large language model (GPT-4o-mini [44]) to evaluate the semantic correctness of the generated answer compared to the ground truth.

### 7.5.2. Baselines

We compared our framework against a diverse set of strong baselines, categorized into three primary groups:

- **Vanilla LLMs:** This category includes standard large language models such as Llama-8B [45], Llama-13B [45], GPT-3.5-turbo [44], and GPT-4o-mini [44], evaluated in a closed-book setting without external retrieval.
- **Standard RAG:** We evaluated standard retrieval-augmented generation approaches using dense retrieval with varying context lengths (Top-1, Top-3, and Top-5 retrieved chunks).

Table 7 | Performance Comparison across different RAG methods

Method	HotpotQA		2WikiMultiHopQA		MuSiQue	
	Contain-Acc.	GPT-Acc.	Contain-Acc.	GPT-Acc.	Contain-Acc.	GPT-Acc.
llama-8B	31.10	27.30	33.60	16.20	7.40	8.10
llama-13B	24.20	16.80	21.90	10.50	3.30	4.40
GPT-3.5-turbo	33.40	43.20	28.70	31.00	10.30	21.90
GPT-4o-mini	38.90	40.20	36.30	31.40	13.60	15.80
Retrieval (Top-1)	46.30	49.10	36.60	31.70	17.80	21.10
Retrieval (Top-3)	53.00	56.00	44.90	39.70	25.10	27.50
Retrieval (Top-5)	55.70	58.60	48.60	43.00	26.10	29.60
KGP	61.50	60.90	31.60	30.00	25.60	30.10
G-retriever	42.20	40.60	46.60	27.10	14.40	15.50
RAPTOR	55.90	58.30	50.10	42.10	23.30	27.40
E <sup>2</sup> GraphRAG	61.00	63.90	54.30	38.10	23.80	26.20
LightRAG	60.30	59.50	55.20	39.00	27.40	28.60
HippoRAG	57.00	59.30	66.10	59.90	29.30	24.10
GFM-RAG	62.70	65.60	66.80	59.60	29.90	34.60
HippoRAG2	62.90	64.30	62.70	55.00	31.00	35.00
<b>Ours</b>	<b>63.50</b>	<b>67.80</b>	<b>67.10</b>	<b>64.80</b>	<b>31.10</b>	<b>36.20</b>

- **Advanced RAG and Graph Methods:** This category encompasses state-of-the-art graph-based and recursive retrieval methods, including KGP [11], G-retriever [46], RAPTOR [10], E<sup>2</sup>GraphRAG [9], LightRAG [5], HippoRAG[6], HippoRAG2[7] and GFM-RAG[8], which utilize sophisticated structures to enhance reasoning.

### 7.5.3. Results and Analysis

The comparative results are presented in Table 7. Our framework (**denoted as Ours**) demonstrates superior performance across the evaluated datasets, validating the effectiveness of the tri-source adaptive retrieval and semantic-anchored knowledge graph.

**Superiority over Vanilla and Standard RAG:** Vanilla LLMs struggle significantly with specific factual queries across all datasets. While incorporating standard retrieval augmentation (e.g., Top-5 chunks) noticeably improves performance, these text-only approaches still lack the structural awareness necessary to handle complex multi-hop dependencies effectively, consistently lagging behind graph-enhanced methods.

**Comparison with Advanced Graph Methods:** Our method consistently demonstrates competitive or superior performance against strong baselines like RAPTOR and LightRAG, as well as recent advanced models like GFM-RAG and HippoRAG2. On datasets like HotpotQA and 2WikiMultiHopQA, while some baselines achieve competitive surface-level string matching, our framework consistently secures the highest GPT-Acc. This distinct advantage in semantic correctness over mere keyword containment demonstrates the robustness of our semantic anchors in capturing true underlying entity relationships and logical reasoning chains.

**Robustness on Complex Datasets:** The MuSiQue dataset presents a significantly higher level of difficulty, causing a sharp performance drop across most baselines, including advanced graph

approaches like LightRAG and E<sup>2</sup>GraphRAG. In contrast, our method maintains strong and robust performance, outperforming these competitors in both containment and semantic accuracy. This resilience indicates that our hierarchical knowledge graph structure effectively bridges the gap between disparate pieces of loosely connected evidence, a crucial capability for the hard multi-hop reasoning required by such complex queries.

## 7.6. Information Extraction Backbone Evaluation

We evaluate our trained model extraction backbone against its own base checkpoint and two substantially larger open-source references to quantify how much of the scaling gap can be closed by task-specific reinforcement learning.

### 7.6.1. Setup

We evaluate on ten English information extraction benchmarks (12,078 test instances in total) covering three regimes: (i) five held-out cross-domain NER datasets that are absent from the training mix, namely CrossNER-AI, CrossNER-Literature, CrossNER-Music, CrossNER-Politics, and CrossNER-Science; (ii) three in-distribution NER benchmarks, CoNLL2003, NCBI, and BC5CDR; and (iii) two relation extraction benchmarks, SciERC and CoNLL04. Decoding is greedy with a 2,048 response token budget. Unlike the training reward, evaluation reports pure task F1 (entity set F1 for NER and relation triple set F1 for RE); the format and JSON terms are excluded so that comparisons are on a common semantic basis. All models are served with identical prompts on a single H200 GPU.

**Baselines.** We compare four models. Qwen3-4B-Instruct and Qwen3-8B serve as open-source base references at the scales immediately at and above our backbone. Qwen3-32B is a substantially larger reference checkpoint (roughly eight times the parameter count of our backbone) and is included to measure how much raw scale buys on these tasks; it is not fine-tuned for information extraction. Our trained model is initialised from Qwen3-4B-Instruct.

### 7.6.2. Main Results

Table 8 reports per-dataset F1 and Table 9 summarises the results by regime. From the results in these tables, our trained model improves over its own base and a larger open-source base. Our trained model improves over the 4B base on every one of the ten benchmarks, and over the 8B base on eight of ten benchmarks. Averaged over the ten datasets, our trained model lifts the 4B backbone by 3.3 F1 points (from 0.5316 to 0.5647) and beats the 8B base by 2.7 points (0.5382 to 0.5647), despite using half of the parameter count of the 8B reference.

**Our model closes the roughly eight times scaling gap to Qwen3-32B and surpasses it on NER.** On the overall average, our model lags the 32B base by only 0.99 F1 points (0.5647 versus 0.5746). Broken down by regime, our model slightly exceeds the 32B base on held-out NER (0.6035 versus 0.6006) and clearly exceeds it on in-distribution NER (0.7280 versus 0.7059, an improvement of 2.2 F1 points). Per dataset, our trained model beats the 32B base on CoNLL2003 (0.7007 versus 0.6400, an improvement of 6.1 F1 points), on BC5CDR (0.7494 versus 0.7214, an improvement of 2.8 F1 points), on CrossNER-Literature (0.5736 versus 0.5419, an improvement of 3.2 F1 points), and on CrossNER-Politics (0.6855 versus 0.6855, a marginal lead at the fourth decimal). These results show that for structured information extraction, a targeted reinforcement learning run can recover most, and in many cases all, of the benefit that comes from raw parameter scaling.

Table 8 | Per-dataset F1 on the information extraction evaluation suite. **Bold** marks the best score in each row. Qwen3-4B, Qwen3-8B, and Qwen3-32B are open-source base checkpoints without fine-tuning. Our 4B backbone is trained by GRPO on IEPile.

Dataset	Task	Qwen3-4B	Qwen3-8B	Qwen3-32B	Ours (4B)
<i>Held out NER (cross domain generalisation)</i>					
CrossNER-AI	NER	0.4862	0.4933	<b>0.5489</b>	<u>0.5400</u>
CrossNER-Literature	NER	0.5462	<u>0.5581</u>	0.5419	<b>0.5736</b>
CrossNER-Music	NER	0.5791	<u>0.5650</u>	<b>0.6059</b>	<u>0.6050</u>
CrossNER-Politics	NER	0.6611	<u>0.6719</u>	<b>0.6855</b>	<b>0.6855</b>
CrossNER-Science	NER	0.5928	<u>0.5984</u>	<b>0.6207</b>	<u>0.6132</u>
<i>In distribution NER</i>					
CoNLL2003	NER	<u>0.6547</u>	0.6396	0.6400	<b>0.7007</b>
NCBI	NER	<u>0.6737</u>	0.7095	<b>0.7563</b>	<u>0.7340</u>
BC5CDR	NER	0.7126	0.7195	<u>0.7214</u>	<b>0.7494</b>
<i>Relation extraction</i>					
SciERC	RE	0.1166	0.0965	<b>0.1485</b>	<u>0.1270</u>
CoNLL04	RE	0.2933	<u>0.3306</u>	<b>0.4768</b>	0.3181
<b>Average over all ten datasets</b>		0.5316	0.5382	<b>0.5746</b>	<u>0.5647</u>

Table 9 | Average F1 by evaluation regime. Our trained backbone exceeds both the 4B and the 8B open-source base on every regime, and exceeds the 32B base on held-out and in-distribution NER, despite having roughly one-eighth of the parameter count. The relation extraction gap to the 32B base is the main remaining limitation.

Regime	Qwen3-4B	Qwen3-8B	Qwen3-32B	Ours
Held out NER (5 sets)	0.5731	0.5773	0.6006	<b>0.6035</b>
In distribution NER (3 sets)	0.6803	0.6895	0.7059	<b>0.7280</b>
Relation extraction (2 sets)	0.2050	0.2136	<b>0.3127</b>	0.2226
<b>Overall (10 sets)</b>	0.5316	0.5382	<b>0.5746</b>	0.5647

**Remaining gap on relation extraction.** From the results above, the 32B base retains a clear lead on relation extraction, especially on CoNLL04 (0.4768 versus 0.3181, a gap of 15.9 F1 points). SciERC is low across the board, at or below 0.15 F1 for every model, reflecting the intrinsic difficulty of fine-grained scientific relation typing. Closing the relation extraction gap will likely require substantially more relation supervision in the training mixture, or targeted schema-conditioned reward shaping.

In this way, one can observe that a compact 4B extraction backbone, trained for roughly one hour of GRPO on a single eight GPU node with a rule based reward, produces an extractor that (i) uniformly outperforms its own base model, (ii) outperforms the next open-source scale on eight of ten benchmarks, and (iii) matches or exceeds a checkpoint eight times larger on held out and on in distribution NER. This makes our model the default extractor in the Agents-K1 pipeline: it delivers the extraction quality of a much larger model at a fraction of the inference cost.

## 8. Conclusion

We presented Agents-K1, an agent-native knowledge orchestration that turns raw documents into scientific knowledge graphs for research agents. Agents-K1 unifies three layers: a KG infrastructure that parses full papers and builds Scholar-KG over 2.46 million scientific papers, with a schema-

adaptive General-KG extension for arbitrary documents; an LLM infrastructure built around a 4B reinforcement-learned extraction backbone; and GraphAnything CLI, an agent-facing interface that connects web search, multimodal graph retrieval, and cross-document traversal. This design turns scholarly knowledge from scattered papers and citation links into reusable, evidence-grounded graph knowledge that agents can retrieve, inspect, and act on. Empirically, Agents-K1 lifts Gemini-3 overall accuracy from 7.9% to 24.6% and GPT-5.2 from 25.2% to 39.4% on the FRONTIERSCIENCE-RESEARCH benchmark, while also improving geoscience research reasoning and multi-hop question answering. Our analysis further supports the central design choice: organizing evidence in connected graphs enables more reliable cross-source reasoning than repeatedly searching separate text fragments. We release a one-million-paper subset of Scholar-KG together with the extraction backbone, aiming to provide the community with a practical knowledge infrastructure for research agents that reason over structured scientific knowledge rather than rebuilding it from raw text at every query.

## References

- [1] Yutaro Yamada et al. “The ai scientist-v2: Workshop-level automated scientific discovery via agentic tree search”. In: *arXiv preprint arXiv:2504.08066* (2025).
- [2] NovelSeek Team et al. “NovelSeek: When Agent Becomes the Scientist—Building Closed-Loop System from Hypothesis to Verification”. In: *arXiv e-prints* (2025), arXiv–2505.
- [3] Shiyang Feng et al. “Internagent-1.5: A unified agentic framework for long-horizon autonomous scientific discovery”. In: *arXiv preprint arXiv:2602.08990* (2026).
- [4] Juraj Gottweis et al. “Towards an AI co-scientist”. In: *arXiv preprint arXiv:2502.18864* (2025).
- [5] Zirui Guo et al. *LightRAG: Simple and Fast Retrieval-Augmented Generation*. 2025. arXiv: [2410.05779](https://arxiv.org/abs/2410.05779) [cs.IR]. URL: <https://arxiv.org/abs/2410.05779>.
- [6] Bernal Jimenez Gutierrez et al. “Hipporag: Neurobiologically inspired long-term memory for large language models”. In: *Advances in Neural Information Processing Systems 37* (2024), pp. 59532–59569.
- [7] Bernal Jiménez Gutiérrez et al. *From RAG to Memory: Non-Parametric Continual Learning for Large Language Models*. 2025. arXiv: [2502.14802](https://arxiv.org/abs/2502.14802) [cs.CL]. URL: <https://arxiv.org/abs/2502.14802>.
- [8] Linhao Luo et al. “GFM-RAG: graph foundation model for retrieval augmented generation”. In: *arXiv preprint arXiv:2502.01113* (2025).
- [9] Yibo Zhao et al. *E<sup>2</sup>GraphRAG: Streamlining Graph-based RAG for High Efficiency and Effectiveness*. 2025. arXiv: [2505.24226](https://arxiv.org/abs/2505.24226) [cs.AI]. URL: <https://arxiv.org/abs/2505.24226>.
- [10] Parth Sarthi et al. *RAPTOR: Recursive Abstractive Processing for Tree-Organized Retrieval*. 2024. arXiv: [2401.18059](https://arxiv.org/abs/2401.18059) [cs.CL]. URL: <https://arxiv.org/abs/2401.18059>.
- [11] Yu Wang et al. *Knowledge Graph Prompting for Multi-Document Question Answering*. 2023. arXiv: [2308.11730](https://arxiv.org/abs/2308.11730) [cs.CL]. URL: <https://arxiv.org/abs/2308.11730>.
- [12] Miles Wang et al. “FrontierScience: Evaluating AI’s Ability to Perform Expert-Level Scientific Tasks”. In: *arXiv preprint arXiv:2601.21165* (2026).
- [13] Zhilin Yang et al. “HotpotQA: A dataset for diverse, explainable multi-hop question answering”. In: *Proceedings of the 2018 conference on empirical methods in natural language processing*. 2018, pp. 2369–2380.
- [14] Xanh Ho et al. “Constructing a multi-hop qa dataset for comprehensive evaluation of reasoning steps”. In: *arXiv preprint arXiv:2011.01060* (2020).

- [15] Harsh Trivedi et al. “MuSiQue: Multihop Questions via Single-hop Question Composition”. In: *Transactions of the Association for Computational Linguistics* 10 (2022), pp. 539–554.
- [16] Yunfan Gao et al. “Retrieval-augmented generation for large language models: A survey”. In: *arXiv preprint arXiv:2312.10997* (2023).
- [17] Yixuan Huang et al. “RaDAR: Relation-aware Diffusion-Asymmetric Graph Contrastive Learning for Recommendation”. In: *Proceedings of the ACM Web Conference 2026*. 2026, pp. 6445–6456.
- [18] Shangheng Du et al. “MLEvolve: A Self-Evolving Framework for Automated Machine Learning Algorithm Discovery”. In: *arXiv preprint arXiv:2606.06473* (2026).
- [19] Zongsheng Cao et al. “Tv-rag: A temporal-aware and semantic entropy-weighted framework for long video retrieval and understanding”. In: *Proceedings of the 33rd ACM International Conference on Multimedia*. 2025, pp. 9071–9079.
- [20] Chi-Min Chan et al. “Rq-rag: Learning to refine queries for retrieval augmented generation”. In: *arXiv preprint arXiv:2404.00610* (2024).
- [21] Zirui Guo et al. “LightRAG: Simple and Fast Retrieval-Augmented Generation”. In: *arXiv preprint arXiv:2410.05779* (2024).
- [22] Hongjin Qian et al. “Memorag: Moving towards next-gen rag via memory-inspired knowledge discovery”. In: *arXiv preprint arXiv:2409.05591* (2024).
- [23] Ritvik Aggarwal Ishneet Sukhvinder Singh Ibrahim Allahverdiyev et al. “ChunkRAG: Novel LLM-Chunk Filtering Method for RAG Systems”. In: *arXiv preprint arXiv:2410.19572* (2024).
- [24] Zongsheng Cao et al. “ViG-RAG: Video-aware Graph Retrieval-Augmented Generation via Temporal and Semantic Hybrid Reasoning”. In: *Proceedings of the AAAI Conference on Artificial Intelligence*. Vol. 40. 1. 2026, pp. 48–56.
- [25] Darren Edge et al. “From local to global: A graph rag approach to query-focused summarization”. In: *arXiv preprint arXiv:2404.16130* (2024).
- [26] Mufei Li, Siqi Miao, and Pan Li. “Simple is effective: The roles of graphs and large language models in knowledge-graph-based retrieval-augmented generation”. In: *arXiv preprint arXiv:2410.20724* (2024).
- [27] Manuel Faysse et al. “Colpali: Efficient document retrieval with vision language models”. In: *arXiv preprint arXiv:2407.01449* (2024).
- [28] Zongsheng Cao et al. “Diffusione: Reasoning on knowledge graphs via diffusion-based graph neural networks”. In: *Proceedings of the 30th ACM SIGKDD Conference on Knowledge Discovery and Data Mining*. 2024, pp. 222–230.
- [29] Junde Wu et al. *Medical Graph RAG: Towards Safe Medical Large Language Model via Graph Retrieval-Augmented Generation*. 2024. arXiv: 2408.04187 [cs.CV]. URL: <https://arxiv.org/abs/2408.04187>.
- [30] Kartik Sharma, Peeyush Kumar, and Yunqing Li. *OG-RAG: Ontology-Grounded Retrieval-Augmented Generation For Large Language Models*. 2024. arXiv: 2412.15235 [cs.CL]. URL: <https://arxiv.org/abs/2412.15235>.
- [31] Lei Liang et al. *KAG: Boosting LLMs in Professional Domains via Knowledge Augmented Generation*. 2024. arXiv: 2409.13731 [cs.CL]. URL: <https://arxiv.org/abs/2409.13731>.
- [32] Tianyu Fan et al. *MiniRAG: Towards Extremely Simple Retrieval-Augmented Generation*. 2025. arXiv: 2501.06713 [cs.AI]. URL: <https://arxiv.org/abs/2501.06713>.
- [33] Jinyu Wang et al. *PIKE-RAG: sPecialized Knowledge and Rationale Augmented Generation*. 2025. arXiv: 2501.11551 [cs.CL]. URL: <https://arxiv.org/abs/2501.11551>.

- [34] Boyu Chen et al. *PathRAG: Pruning Graph-based Retrieval Augmented Generation with Relational Paths*. 2025. arXiv: [2502.14902](https://arxiv.org/abs/2502.14902) [cs.CL]. URL: <https://arxiv.org/abs/2502.14902>.
- [35] Bernal Jiménez Gutiérrez et al. *From RAG to Memory: Non-Parametric Continual Learning for Large Language Models*. 2025. arXiv: [2502.14802](https://arxiv.org/abs/2502.14802) [cs.CL]. URL: <https://arxiv.org/abs/2502.14802>.
- [36] Yusong Hu et al. “FlowSearch: Advancing deep research with dynamic structured knowledge flow”. In: *arXiv preprint arXiv:2510.08521* (2025).
- [37] Shangheng Du et al. “AutoMLGen: Navigating Fine-Grained Optimization for Coding Agents”. In: *arXiv preprint arXiv:2510.08511* (2025).
- [38] Tongyi DeepResearch Team et al. “Tongyi deepresearch technical report”. In: *arXiv preprint arXiv:2510.24701* (2025).
- [39] Xiaoxi Li et al. “Webthinker: Empowering large reasoning models with deep research capability”. In: *arXiv preprint arXiv:2504.21776* (2025).
- [40] Jinxin Shi et al. “DualResearch: Entropy-Gated Dual-Graph Retrieval for Answer Reconstruction”. In: *arXiv preprint arXiv:2510.08959* (2025).
- [41] OpenAI. *DeepResearch*. <https://openai.com/research/deep-research>. Accessed: 2025-09-24. 2025.
- [42] Google DeepMind. *Gemini Deep Research*. <https://deepmind.google/technologies/gemini/deep-research/>. Accessed: 2025-09-24. 2024.
- [43] DeepSeek-AI et al. *DeepSeek-V3 Technical Report*. 2025. arXiv: [2412.19437](https://arxiv.org/abs/2412.19437) [cs.CL]. URL: <https://arxiv.org/abs/2412.19437>.
- [44] OpenAI et al. *GPT-4 Technical Report*. 2024. arXiv: [2303.08774](https://arxiv.org/abs/2303.08774) [cs.CL]. URL: <https://arxiv.org/abs/2303.08774>.
- [45] Aaron Grattafiori et al. *The Llama 3 Herd of Models*. 2024. arXiv: [2407.21783](https://arxiv.org/abs/2407.21783) [cs.AI]. URL: <https://arxiv.org/abs/2407.21783>.
- [46] Xiaoxin He et al. *G-Retriever: Retrieval-Augmented Generation for Textual Graph Understanding and Question Answering*. 2024. arXiv: [2402.07630](https://arxiv.org/abs/2402.07630) [cs.LG]. URL: <https://arxiv.org/abs/2402.07630>.

## Appendix

### A. Citation Context Classification Schema

To precisely quantify the intellectual lineage and contextual dependency of the referenced literature, we formulate the citation analysis as a fine-grained classification task. Each citation mention extracted from the full text is categorized into one of five hierarchical levels based on its contextual significance and direct impact on the proposed research. The scoring rubric is defined as follows:

**Level 5: Foundational Citation.** The current research is inextricably built upon this prior work. Without this reference, the core theory, model, or methodology of the paper would lack its foundational basis. Typical contextual markers include phrases such as “*We build upon...*” or “*Following the methodology of...*”.

**Level 4: Strong Citation.** The referenced work serves as a primary pillar of support or a critical benchmark. It directly influences the study’s experimental design, validation, or conclusions. Contextual markers often include “*As demonstrated by...*” or “*We compare our framework against...*”.

**Level 3: Moderate Citation.** The citation provides supporting background, empirical evidence, or conceptual inspiration, yet it does not constitute the absolute core foundation. It is frequently utilized to justify the research motivation or establish theoretical associations (e.g., “*Inspired by...*” or “*Consistent with findings in...*”).

**Level 2: Contextual Citation.** The reference is utilized primarily to map the broader research landscape or delineate related work. The direct methodological link to the current study is relatively weak, commonly appearing in comprehensive literature reviews (e.g., “*Several recent studies have explored...*”).

**Level 1: Peripheral Citation.** The work is mentioned strictly for academic breadth, historical context, or general overview, exerting no substantive impact on the paper’s core logic (e.g., “*For a general overview, see...*”).

**Aggregation Strategy** Given that a single reference may be cited multiple times across different sections of a manuscript, we apply a max-pooling aggregation strategy. Specifically, the definitive classification for a given reference is determined by the maximum score it achieves across all its mentions within the text. Furthermore, references that are listed in the bibliography but lack explicit in-text mentions are conservatively assigned a default score of Level 1 (Peripheral Citation) to prevent logical anomalies in the final reference graph. For quantitative aggregation, each level is explicitly assigned a corresponding integer score ranging from 5 (Foundational) to 1 (Peripheral).

### B. Proofs and Constructive Details for Section 4.5

This appendix gives the projection rules used in the proofs, the proofs of Propositions 1, 2, and 3, and the witness construction that certifies the strict gap term of (8). We keep the notation of Section 4.5: a payload is  $\mathcal{P}_D = (\mathcal{V}, \mathcal{E}_h)$ , and every view is identifier preserving on  $\mathcal{V}$ .

#### B.1. Projection Rules

For a hyperedge  $e = (v_1, \dots, v_k) \in \mathcal{E}_h$ , write  $|e| = k$  and  $\text{set}(e) = \{v_1, \dots, v_k\}$ . The two views invoked in the proofs below are:

- **Binary view**  $\Phi_b$ . Keep only arity-2 edges:  $\Phi_b(\mathcal{P}_D) = (\mathcal{V}, \{e \in \mathcal{E}_h : |e| = 2\})$ .

- **$N$ -ary view  $\Phi_n$ .** Keep  $\{e \in \mathcal{E}_h : |e| \geq 3\}$  and add hyperedges produced by the upgrade operator  $U_n$  from the binary skeleton, where  $U_n$  promotes any clique whose pairwise edges share a chunk to a single hyperedge.

The temporal, person, event, DIY, and scientific-KG views are described in Section 4.3 and Section 4.1; each is a deterministic projection on the same  $\mathcal{V}$ , so the arguments below apply to them without modification.

## B.2. Proof of Proposition 1 (Identifier Preserving Joins)

**Upper bound.**  $\Phi_u(\mathcal{P}_D)$  and  $\Phi_v(\mathcal{P}_D)$  live over the same  $\mathcal{V}$  with identical identifiers. Build a hash table on  $\Phi_u \upharpoonright K$  keyed by node identifier in  $O(|K|)$  time, then for each  $v \in K \cap \Phi_v$  look up  $H_u[v]$  in expected  $O(1)$ . The total cost is  $O(|K|)$ , and matches are exact because identifiers compare by equality.

**Lower bound.** If the two pipelines produce  $\mathcal{V}_u \cap \mathcal{V}_v = \emptyset$ , no shared key is available and alignment must rely on a per-pair surface-form similarity test  $\text{sim}(u, v)$ . Without a blocking key or metric structure, all  $|\mathcal{V}_u| \cdot |\mathcal{V}_v|$  pairs must be considered in the worst case, giving  $\Omega(|\mathcal{V}_u| \cdot |\mathcal{V}_v|)$ .

**False merge probability.** Let  $\sigma(v)$  denote the surface form of node  $v$ , and let  $H = \{v \in \mathcal{V} : |\sigma^{-1}(\sigma(v))| \geq 2\}$  be the homonym set. If  $H$  is empty, there is no surface-form homonym to merge. Otherwise, sample  $v \sim \text{Unif}(H)$  and a uniform target  $w \sim \text{Unif}(\mathcal{V})$ . For each  $v \in H$ , there are  $|\sigma^{-1}(\sigma(v))| - 1$  wrong targets with the same surface form. Averaging over  $H$  gives (6). A matcher that merges identical surface forms therefore has this probability of selecting a spurious merge target under the same sampling model. Shared identifiers do not remove homonyms from the text; they avoid this error because joins compare identifiers rather than  $\sigma(v)$ . Thus the surface-form false-merge probability is zero for ID-based joins.  $\square$

## B.3. Proof of Proposition 2 (Cross View Reachability)

**(1) Monotonicity.** Every view shares  $\mathcal{V}$  and contributes its edges to  $\mathcal{E}_U$ , so any  $h$ -hop walk in  $\Phi_v(\mathcal{P}_D)$  is also an  $h$ -hop walk in  $\mathcal{P}_U$ .

**(2) Strict gap.** Pick a query  $q$  and a gold hyperedge  $e = (v_1, \dots, v_k) \in H_{\geq 3}^{(h)}(q)$  with  $k \geq 3$ . The binary view  $\Phi_b$  discards  $e$  entirely; the  $n$ -ary view  $\Phi_n$  exposes all  $k$  endpoints in one hop. For each such  $e$ , let  $B_e$  be the endpoints of  $e$  that are reachable from  $S(q)$  only through  $e$  and are not retained by the binary view. Every node in  $\bigcup_e B_e$  is reachable in  $\mathcal{P}_U$  and not reachable in  $\Phi_b(\mathcal{P}_D)$ , which gives (7). In the two-anchor witness used below,  $B_e = \text{set}(e) \setminus \{v_a, v_b\}$ ; if these hidden endpoint sets are disjoint across gold hyperedges, the bound reduces to  $\sum_e (|e| - 2)$ .

**(3) Hardness.** The main text only uses the monotonicity and strict-gap parts of Proposition 2. For completeness, we also record why a compact hyperedge explanation cannot in general be recovered cheaply from the binary projection alone. We reduce from EDGE-CLIQUE-COVER (ECC), which asks whether the edges of a graph  $G$  admit a cover by at most  $k$  cliques. Define HYPER-RECOVER( $G_b, k$ ) as the decision problem that asks whether a binary graph  $G_b$  is the clique expansion of at most  $k$  hyperedges of arity at least two. Given an ECC instance  $(G, k)$ , set  $G_b := G$  and ask HYPER-RECOVER( $G_b, k$ ). A YES instance is exactly an edge clique cover of  $G$  of size  $\leq k$ , because each hyperedge induces one clique and each clique in the cover can be represented as one hyperedge. The reduction is polynomial, so exact minimum recovery under this projection model is NP-hard.  $\square$

#### B.4. Proof of Proposition 3 (Candidate Coverage)

For any single view  $v$ , edge monotonicity of  $\Phi_R$  gives  $\Phi_R(\mathcal{P}_U, q) \supseteq \Phi_R(\Phi_v(\mathcal{P}_D), q)$  before final ranking and truncation. Therefore the gold candidates retrieved by the best single view are also retrieved by the union view. The extra gold candidates counted by  $\Delta_h(q)$  are, by definition, outside every single-view candidate set, so the two contributions are disjoint:

$$|\Phi_R(\mathcal{P}_U, q) \cap A_h^*(q)| \geq \max_v |\Phi_R(\Phi_v(\mathcal{P}_D), q) \cap A_h^*(q)| + |A_h^*(q) \cap (\Phi_R(\mathcal{P}_U, q) \setminus \bigcup_v \Phi_R(\Phi_v(\mathcal{P}_D), q))|.$$

Dividing by  $|A_h^*(q)|$  yields (8). The Scholar-KG case follows because its view is also identifier preserving on the same  $\mathcal{V}$ , so it contributes another summand to the union without renaming nodes.  $\square$

#### B.5. Witness Construction for the Strict-Gap Term

The following procedure instantiates a query for which  $\Delta_h(q)$  in (8) is strictly positive: (i) pick a hyperedge  $e \in \mathcal{E}_h$  with  $|e| \geq 3$  that carries a nonempty qualifier  $\kappa(e)$ ; (ii) choose two endpoints  $v_a, v_b \in \text{set}(e)$  as anchors; (iii) form the query “which entities appear with  $v_a$  and  $v_b$  under qualifier  $\kappa(e)$ ?”. The gold answer set is  $\text{set}(e) \setminus \{v_a, v_b\}$ . The binary view drops the bundled edge  $e$ ; the temporal bundled view  $\Phi_t \circ \Phi_n$  exposes  $\text{set}(e)$  in a single hop. Therefore, for this query family, the union view retrieves gold candidates that the binary view does not expose. Iterating over  $\mathcal{E}_h^{\geq 3}$  generates the witness corpus used in Section 7.

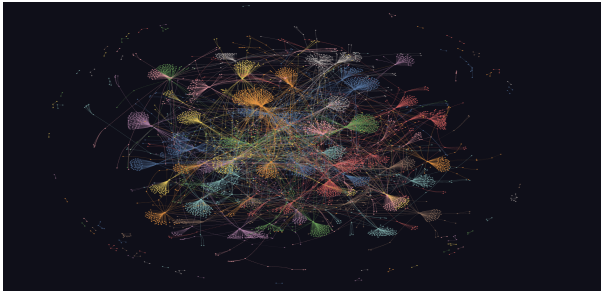
### C. Knowledge Graph Visualization

To provide comprehensive insight into the constructed knowledge network, Figure 6 illustrates a hierarchical breakdown of the extracted subgraphs. Progressively zooming from a macroscopic community structure down to influential focal nodes and specific relational triplets, the visualization highlights our framework’s fine-grained parsing capabilities. The densely populated edges denote heterogeneous relationships that integrate the network across multiple granularities: document citations (Paper  $\rightarrow$  Paper), methodological groundings (Paper  $\rightarrow$  Content), and semantic dependencies (Content  $\rightarrow$  Content). Together, these links weave isolated scientific literature into a unified reasoning space.

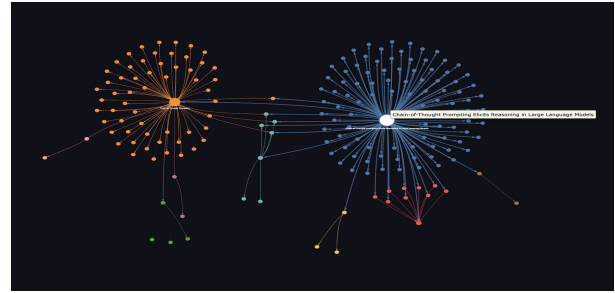
To further elucidate the extraction capabilities demonstrated in Figure 6, we provide a detailed examination of the focal node representing the seminal “Chain-of-Thought Prompting” (CoT) paper. While subfigures (a) and (b) contextualize the document within the macroscopic topology, subfigures (c) through (f) systematically break down the extracted relational triplets according to our proposed modular taxonomy.

Specifically, **Module A** (Figure 6c) handles explicit meta-factual attributes, accurately anchoring the document to its real-world entities (e.g., the author, Jason Wei). Moving into the semantic content of the PDF, **Module B** (Figure 6d) captures textually explicit entities, correctly identifying that the document *proposes* the “CoT Prompting” methodology. Beyond surface-level extraction, **Module C** (Figure 6e) highlights the framework’s advanced natural language understanding by extracting implicit or abstracted entities. It deduces that the paper’s *involved\_task* is “Symbolic Reasoning”—an abstraction that requires synthesizing the paper’s core contributions rather than merely executing exact keyword matching.

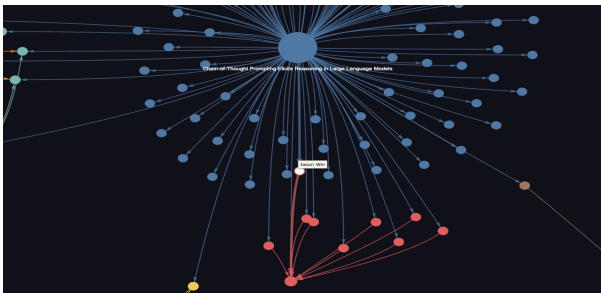
Furthermore, while **Module D** (Figure 6f) preserves traditional document-level structural integrity by mapping explicit citation relationships (Paper  $\rightarrow$  Paper), our framework fundamentally transcends these document boundaries. As shown in Figure 6(g), it reveals deep technical dependencies within the semantic space (Content  $\rightarrow$  Content), recognizing that the CoT concept explicitly *implements* “few-shot prompting.”



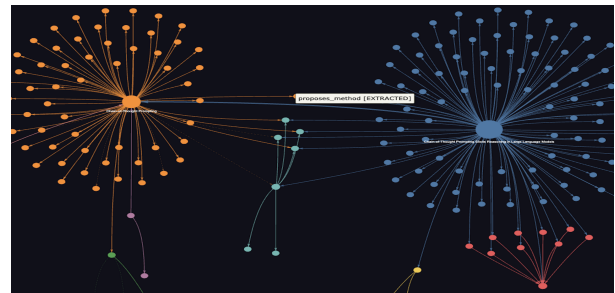
(a) Macroscopic view of 30 seminal papers



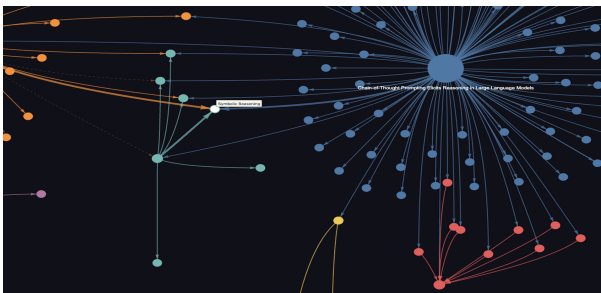
(b) Focal Paper Node: “Chain-of-Thought Prompting Elicits Reasoning in Large Language Models”(CoT)



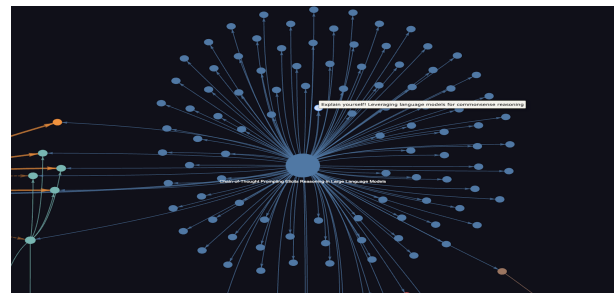
(c) Paper  $\rightarrow$  Content: CoT  $\xrightarrow{\text{authored\_by}}$  Jason Wei  
(Module A: Meta/Factual Entities)



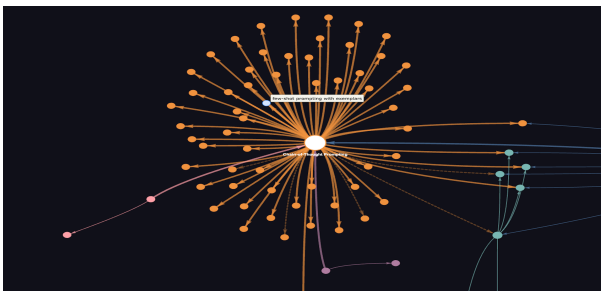
(d) Paper  $\rightarrow$  Content: CoT  $\xrightarrow{\text{proposes}}$  CoT Prompting  
(Module B: Textually Mentioned Entities)



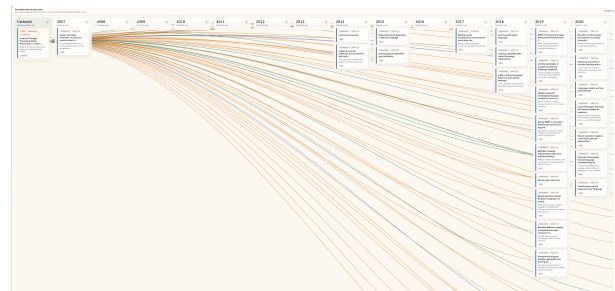
(e) Paper  $\rightarrow$  Content:  
CoT  $\xrightarrow{\text{involved\_task}}$  Symbolic Reasoning  
(Module C: Implicit/Abstracted Entities)



(f) Paper  $\rightarrow$  Paper:  
CoT  $\xrightarrow{\text{cites}}$  “Explain yourself! Leveraging language models for commonsense reasoning”  
(Module D: Citation Relationships)



(g) Content  $\rightarrow$  Content:  
CoT  $\xrightarrow{\text{implements}}$  few-shot prompting



(h) Temporal Evolution: Longitudinal timeline of CoT citations

Figure 6 | Comprehensive, multi-dimensional visualization of the knowledge network. Subfigures (a)–(b) present the global topology and focal nodes. Subfigures (c)–(g) explicitly detail the rich variety of extracted semantic triplets, covering authorship, methodological claims, involved tasks, document citations, and technical implementations. Finally, subfigure (h) maps the focal paper’s citation network onto a longitudinal temporal timeline.

Finally, because scientific knowledge is inherently dynamic, Figure 6(h) projects the focal paper’s citation network onto a longitudinal temporal axis. This temporal evolution graph illustrates the developmental trajectory and subsequent academic impact of the CoT methodology. Collectively, this multi-level breakdown validates that our framework does not merely parse text into isolated nodes; rather, it fully reconstructs the underlying scientific reasoning process into a structured, navigable, and temporally-aware knowledge infrastructure.

## D. Disaggregated Knowledge Graph Schema

To ensure full transparency and provide a comprehensive view of the extraction schema, the complete raw JSON representation of the generated knowledge graph is presented below. This structured data encompasses meta-factual entities, textually mentioned entities, implicitly abstracted variables, and complex relational edges.

### Knowledge Graph Entity and Relation Extraction (JSON)

```

1 {
2   "A_Meta_Factual_Entities": {
3     "Paper": {
4       "title": "Adam: A Method for Stochastic Optimization",
5       "pub_year": "2014",
6       "type": "research paper",
7       "language": "English"
8     },
9     "Authors": [
10      {
11        "name": "Jimmy Ba",
12        "ordering": 0,
13        "corresponding_flag": false
14      },
15      {
16        "name": "Diederik P. Kingma",
17        "ordering": 1,
18        "corresponding_flag": false
19      }
20    ]
21  },
22  "B_Textually_Mentioned_Entities": {
23    "Tasks": [
24      {
25        "name": "Stochastic Optimization",
26        "type": "optimization",
27        "input_modality": "stochastic objective function gradients",
28        "output_modality": "optimized parameters",
29        "constraints": "high-dimensional parameter spaces, noisy/sparse gradients",
30        "aliases": [
31          "stochastic gradient descent",
32          "adaptive optimization"
33        ]
34      }
35    ],
36    "Methods": [
37      {
38        "name": "Adam",
39        "proposed_or_cited": "proposed",
40        "components": [
41          "adaptive moment estimation",
42          "bias correction",
43          "exponential moving averages"
44        ],
45        "training_objectives": [
46          "minimize expected value of stochastic objective function"
47        ],
48        "inference_strategies": [
49          "parameter updates using bias-corrected moment estimates"
50        ]
51      }
52    ]
53  }
54 }

```

```

51     "aliases": [
52         "adaptive moment estimation",
53         "Adam optimizer"
54     ]
55 },
56 {
57     "name": "AdaGrad",
58     "proposed_or_cited": "cited",
59     "components": [
60         "adaptive learning rates for sparse gradients"
61     ],
62     "training_objectives": [
63         "optimize sparse gradient problems"
64     ],
65     "inference_strategies": [
66         "diagonal rescaling of gradients"
67     ],
68     "aliases": [
69         "Adaptive Gradient Algorithm"
70     ]
71 },
72 {
73     "name": "RMSProp",
74     "proposed_or_cited": "cited",
75     "components": [
76         "moving average of squared gradients"
77     ],
78     "training_objectives": [
79         "handle non-stationary objectives"
80     ],
81     "inference_strategies": [
82         "divide gradient by running average of magnitudes"
83     ],
84     "aliases": [
85         "Root Mean Square Propagation"
86     ]
87 },
88 {
89     "name": "AdaMax",
90     "proposed_or_cited": "proposed",
91     "components": [
92         "infinity norm variant of Adam"
93     ],
94     "training_objectives": [
95         "simplify Adam's bias correction"
96     ],
97     "inference_strategies": [
98         "use L-infinity norm for moment estimation"
99     ],
100     "aliases": [
101         "Adaptive Moment Estimation with Infinity Norm"
102     ]
103 }
104 ],
105 "Metrics": [
106     {
107         "full_name": "Regret Bound",
108         "abbreviation": "Regret",
109         "formula": "sum_{t=1}^T [f_t(theta_t) - f_t(theta^*)]"
110     }
111 ],
112 "Baselines": [
113     {
114         "name": "AdaGrad",
115         "strong_baseline": true
116     },
117     {
118         "name": "RMSProp",
119         "strong_baseline": true
120     }

```

```

121 ],
122 "Implementation": {
123   "learning_rate": "0.001"
124 },
125 "Theorems": [
126   {
127     "number": "4.1",
128     "statement": "Adam achieves  $O(\sqrt{T})$  regret bound under bounded gradients
129       and parameter constraints",
130     "premises": "Bounded gradients, bounded parameter distances,  $\beta_1/\sqrt{(\beta_2)} < 1$ ",
131     "conclusion": "Regret bound comparable to best known results in online
132       convex optimization"
133   }
134 ],
135 "Figures_Tables": [
136   {
137     "type": "algorithm",
138     "number": "1",
139     "caption": "Adam: Proposed algorithm for stochastic optimization",
140     "content_summary": "Pseudocode for Adam optimizer with bias-corrected moment
141       estimates"
142   }
143 ],
144 "Domain_Terms": [
145   {
146     "term": "Signal-to-Noise Ratio (SNR)",
147     "standard_name": "SNR",
148     "definition": "Ratio of estimated first moment to square root of estimated
149       second moment ( $m_{\hat{t}} / \sqrt{v_{\hat{t}}}$ )"
150   },
151   {
152     "term": "Bias-Corrected Moment Estimates",
153     "standard_name": "Bias Correction",
154     "definition": "Adjustment of initial moment estimates to counteract zero
155       initialization bias ( $m_{\hat{t}} = m_t / (1-\beta_1^t)$ ,  $v_{\hat{t}} = v_t / (1-\beta_2^t)$ )"
156   }
157 ],
158 "C_Implicit_Abstracted_Entities": {
159   "Problem_Definition": {
160     "input_space": "Stochastic objective function  $f(\theta)$  with parameters  $\theta$ ",
161     "output_space": "Optimized parameter vector  $\theta_t$  minimizing  $E[f(\theta)]$ ",
162     "constraints": [
163       "High-dimensional parameter spaces",
164       "Noisy/sparse gradients",
165       "Non-stationary objectives"
166     ],
167     "assumptions": [
168       "Differentiable objective function",
169       "Bounded gradients",
170       "Exponentially decaying moment estimates"
171     ]
172   },
173   "Motivation": {
174     "existing_limitations": [
175       "AdaGrad's poor performance on non-stationary objectives",
176       "RMSProp's lack of bias correction for initial moments",
177       "SGD's sensitivity to learning rate scheduling"
178     ],
179     "gap_categories": [
180       "Need for adaptive learning rates with bias correction",
181       "Combining strengths of AdaGrad and RMSProp",
182       "Handling sparse gradients in non-stationary environments"
183     ]
184   },
185   "Contributions": {
186     "main_contributions": [
187       "Proposed Adam optimizer combining AdaGrad and RMSProp advantages",

```

```

184     "Theoretical analysis of  $O(\sqrt{T})$  regret bound",
185     "Bias correction technique for moment estimates",
186     "AdaMax variant using infinity norm"
187 ],
188 "component_alignment": [
189     "Adaptive learning rates -> AdaGrad/RMSProp combination",
190     "Bias correction -> Theoretical convergence guarantees",
191     "Regret analysis -> Online convex optimization framework"
192 ],
193 },
194 "Hypotheses": [
195     {
196         "hypothesis": "Adam's adaptive learning rates with bias correction will
197             outperform existing methods on non-stationary objectives",
198         "testable": true,
199         "scope": "High-dimensional stochastic optimization problems"
200     }
201 ],
202 "Findings": {
203     "quantitative": [
204         "Empirical results show Adam consistently outperforms other methods",
205         "Regret bound matches best known  $O(\sqrt{T})$  results"
206     ],
207     "qualitative": [
208         "Automatic step size annealing through SNR mechanism",
209         "Invariance to gradient rescaling improves robustness"
210     ]
211 },
212 "Explanations": [
213     {
214         "phenomenon": "Adam's convergence guarantees",
215         "explanation": "Theoretical analysis shows regret bound depends on gradient
216             norms and parameter distances, with adaptive scaling reducing effective
217             step sizes when SNR is low",
218         "type": "theoretical"
219     }
220 ],
221 "Limitations": {
222     "generalizability": [
223         "Assumes bounded gradients and parameter distances",
224         "Theoretical analysis limited to convex objectives"
225     ],
226     "computational_cost": [
227         "Requires storage of first and second moment vectors"
228     ]
229 },
230 "Design_Rationales": [
231     "Bias correction addresses initial moment estimates being zero-biased",
232     "Exponential moving averages balance recent and historical gradient
233         information",
234     "Signal-to-noise ratio mechanism provides automatic step size annealing"
235 ],
236 "Future_Work": [
237     "Extending to non-convex optimization settings",
238     "Developing variants with improved memory efficiency",
239     "Analyzing performance on specific application domains"
240 ],
241 "Error_Analysis": {
242     "failure_types": [
243         "Large initial steps when  $\beta_2$  is small without bias correction",
244         "Suboptimal convergence when SNR is persistently low"
245     ]
246 },
247 "D_Reference": {
248     "Natural gradient works efficiently in learning": {
249         "cite_type": "Moderate Cite",
250         "related": "The work provides supporting background, as it is referenced to
251             explain the concept of natural gradient descent in relation to Adam.",
252         "evidence": [

```

```

249     3
250 ],
251 "pub_time": 1998,
252 "authors": [
253     "Amari, Shun-Ichi"
254 ],
255 "source": "Neural computation"
256 },
257 "Recent advances in deep learning for speech research at microsoft": {
258     "cite_type": "Moderate Cite",
259     "related": "Provides supporting background or inspiration, used to illustrate
260         the impact of SGD in deep learning success stories.",
261     "evidence": [
262         3
263     ],
264     "pub_time": 2013,
265     "authors": [
266         "Deng, Li",
267         "Li, Jinyu",
268         "Huang, Jui-Ting",
269         "Yao, Kaisheng",
270         "Yu, Dong",
271         "Seide, Frank",
272         "Selter, Michael",
273         "Zweig, Geoff",
274         "He, Xiaodong",
275         "Williams, Jason"
276     ],
277     "source": "ICASSP 2013"
278 },
279 "Adaptive subgradient methods for online learning and stochastic optimization":
280 {
281     "cite_type": "Strong Cite",
282     "related": "The work is a main support as the method combines its advantages
283         for sparse gradients.",
284     "evidence": [
285         4,
286         4,
287         3,
288         4,
289         4,
290         3,
291         3
292     ],
293     "pub_time": 2011,
294     "authors": [
295         "Duchi, John",
296         "Hazan, Elad",
297         "Singer, Yoram"
298     ],
299     "source": "The Journal of Machine Learning Research"
300 },
301 "Generating sequences with recurrent neural networks": {
302     "cite_type": "Moderate Cite",
303     "related": "Provides supporting background on related optimization methods.",
304     "evidence": [
305         3,
306         3
307     ],
308     "pub_time": 2013,
309     "authors": [
310         "Graves, Alex"
311     ],
312     "source": "arXiv preprint arXiv:1308.0850"
313 },
314 "Speech recognition with deep recurrent neural networks": {
315     "cite_type": "Moderate Cite",
316     "related": "Provides supporting background or inspiration, used to illustrate
317         the impact of SGD in deep learning success stories.",
318     "evidence": [

```

```

315     3
316 ],
317 "pub_time": 2013,
318 "authors": [
319     "Graves, Alex",
320     "Mohamed, Abdel-rahman",
321     "Hinton, Geoffrey"
322 ],
323 "source": "In Acoustics, Speech and Signal Processing (ICASSP), 2013 IEEE
324     International Conference on"
325 },
326 "Reducing the dimensionality of data with neural networks": {
327     "cite_type": "Moderate Cite",
328     "related": "Provides supporting background or inspiration, used to illustrate
329         the impact of SGD in deep learning success stories.",
330     "evidence": [
331         3
332     ],
333     "pub_time": 2006,
334     "authors": [
335         "Hinton, G.E.",
336         "Salakhutdinov, R.R."
337     ],
338     "source": "Science"
339 },
340 "Deep neural networks for acoustic modeling in speech recognition: The shared
341     views of four research groups": {
342     "cite_type": "Moderate Cite",
343     "related": "Provides supporting background or inspiration, used to illustrate
344         the impact of SGD in deep learning success stories.",
345     "evidence": [
346         3
347     ],
348     "pub_time": 2012,
349     "authors": [
350         "Hinton, Geoffrey",
351         "Deng, Li",
352         "Yu, Dong",
353         "Dahl, George E",
354         "Mohamed, Abdel-rahman",
355         "Jaitly, Navdeep",
356         "Senior, Andrew",
357         "Vanhoucke, Vincent",
358         "Nguyen, Patrick",
359         "Sainath, Tara N"
360     ],
361     "source": "Signal Processing Magazine, IEEE"
362 },
363 "Improving neural networks by preventing co-adaptation of feature detectors": {
364     "cite_type": "Moderate Cite",
365     "related": "Provides supporting background or inspiration, used to illustrate
366         additional sources of noise in objectives.",
367     "evidence": [
368         3
369     ],
370     "pub_time": 2012,
371     "authors": [
372         "Hinton, Geoffrey E",
373         "Srivastava, Nitish",
374         "Krizhevsky, Alex",
375         "Sutskever, Ilya",
376         "Salakhutdinov, Ruslan R"
377     ],
378     "source": "arXiv preprint arXiv:1207.0580"
379 },
380 "Auto-Encoding Variational Bayes": {
381     "cite_type": "Strong Cite",
382     "related": "The work is a main support or benchmark, as the paper uses the
383         same VAE architecture described in this work for training.",
384     "evidence": [

```

```

379     4
380 ],
381 "pub_time": 2013,
382 "authors": [
383     "Kingma, Diederik P",
384     "Welling, Max"
385 ],
386 "source": "In The 2nd International Conference on Learning Representations (
387     ICLR)"
388 },
389 "Imagenet classification with deep convolutional neural networks": {
390     "cite_type": "Moderate Cite",
391     "related": "Provides supporting background or inspiration, used to illustrate
392         the impact of SGD in deep learning success stories.",
393     "evidence": [
394         3
395     ],
396     "pub_time": 2012,
397     "authors": [
398         "Krizhevsky, Alex",
399         "Sutskever, Ilya",
400         "Hinton, Geoffrey E"
401     ],
402     "source": "In Advances in neural information processing systems"
403 },
404 "Learning word vectors for sentiment analysis": {
405     "cite_type": "Strong Cite",
406     "related": "The dataset from this work is directly used in the experiments,
407         making it a key benchmark for the study.",
408     "evidence": [
409         4
410     ],
411     "pub_time": 2011,
412     "authors": [
413         "Maas, Andrew L",
414         "Daly, Raymond E",
415         "Pham, Peter T",
416         "Huang, Dan",
417         "Ng, Andrew Y",
418         "Potts, Christopher"
419     ],
420     "source": "In Proceedings of the 49th Annual Meeting of the Association for
421         Computational Linguistics: Human Language Technologies-Volume 1"
422 },
423 "Non-asymptotic analysis of stochastic approximation algorithms for machine
424     learning": {
425     "cite_type": "Strong Cite",
426     "related": "The work is a main support, as it demonstrates the improvement of
427         convergence using Polyak-Ruppert averaging.",
428     "evidence": [
429         4
430     ],
431     "pub_time": 2011,
432     "authors": [
433         "Moulines, Eric",
434         "Bach, Francis R"
435     ],
436     "source": "In Advances in Neural Information Processing Systems"
437 },
438 "Revisiting natural gradient for deep networks": {
439     "cite_type": "Moderate Cite",
440     "related": "The work provides supporting background, as it is referenced to
441         explain the Fisher information matrix approximation used in Adam.",
442     "evidence": [
443         3
444     ],
445     "pub_time": 2013,
446     "authors": [
447         "Pascanu, Razvan",
448         "Bengio, Yoshua"
449     ]
450 }

```

```

442 ],
443 "source": "arXiv preprint arXiv:1301.3584"
444 },
445 "Acceleration of stochastic approximation by averaging": {
446 "cite_type": "Strong Cite",
447 "related": "The work is a main support, as it introduces the Polyak-Ruppert
averaging method discussed in the text.",
448 "evidence": [
449 4
450 ],
451 "pub_time": 1992,
452 "authors": [
453 "Polyak, Boris T",
454 "Juditsky, Anatoli B"
455 ],
456 "source": "SIAM Journal on Control and Optimization"
457 },
458 "A fast natural newton method": {
459 "cite_type": "Moderate Cite",
460 "related": "Provides supporting background on related optimization methods.",
461 "evidence": [
462 3
463 ],
464 "pub_time": 2010,
465 "authors": [
466 "Roux, Nicolas L",
467 "Fitzgibbon, Andrew W"
468 ],
469 "source": "In Proceedings of the 27th International Conference on Machine
Learning (ICML-10)"
470 },
471 "Efficient estimations from a slowly convergent robbins-monro process": {
472 "cite_type": "Strong Cite",
473 "related": "The work is a main support, as it introduces the Polyak-Ruppert
averaging method discussed in the text.",
474 "evidence": [
475 4
476 ],
477 "pub_time": 1988,
478 "authors": [
479 "Ruppert, David"
480 ],
481 "source": "Technical report, Cornell University Operations Research and
Industrial Engineering"
482 },
483 "No more pesky learning rates": {
484 "cite_type": "Moderate Cite",
485 "related": "Provides supporting background on related optimization methods.",
486 "evidence": [
487 3
488 ],
489 "pub_time": 2012,
490 "authors": [
491 "Schaul, Tom",
492 "Zhang, Sixin",
493 "LeCun, Yann"
494 ],
495 "source": "arXiv preprint arXiv:1206.1106"
496 },
497 "Fast large-scale optimization by unifying stochastic gradient and quasi-newton
methods": {
498 "cite_type": "Strong Cite",
499 "related": "The work is a main support or benchmark, as the paper compares
Adam's memory requirements to those of SFO.",
500 "evidence": [
501 4,
502 4
503 ],
504 "pub_time": 2014,
505 "authors": [

```

```

506     "Sohl-Dickstein, Jascha",
507     "Poole, Ben",
508     "Ganguli, Surya"
509 ],
510 "source": "In Proceedings of the 31st International Conference on Machine
      Learning (ICML-14)"
511 },
512 "On the importance of initialization and momentum in deep learning": {
513   "cite_type": "Moderate Cite",
514   "related": "The work provides supporting evidence for the importance of
      decaying the momentum coefficient, but is not central to the paper's core
      theory.",
515   "evidence": [
516     3
517   ],
518   "pub_time": 2013,
519   "authors": [
520     "Sutskever, Ilya",
521     "Martens, James",
522     "Dahl, George",
523     "Hinton, Geoffrey"
524   ],
525   "source": "In Proceedings of the 30th International Conference on Machine
      Learning (ICML-13)"
526 },
527 "Lecture 6.5 - RMSProp": {
528   "cite_type": "Strong Cite",
529   "related": "The work is a main support as the method combines its advantages
      for on-line and non-stationary settings.",
530   "evidence": [
531     4,
532     3,
533     4,
534     4,
535     3,
536     3
537   ],
538   "pub_time": 2012,
539   "authors": [
540     "Tieleman, T.",
541     "Hinton, G."
542   ],
543   "source": "COURSERA: Neural Networks for Machine Learning"
544 },
545 "Fast dropout training": {
546   "cite_type": "Moderate Cite",
547   "related": "The paper uses a suggestion from this work as background for
      applying dropout noise during training.",
548   "evidence": [
549     3
550   ],
551   "pub_time": 2013,
552   "authors": [
553     "Wang, Sida",
554     "Manning, Christopher"
555   ],
556   "source": "In Proceedings of the 30th International Conference on Machine
      Learning (ICML-13)"
557 },
558 "Adadelta: An adaptive learning rate method": {
559   "cite_type": "Moderate Cite",
560   "related": "Provides supporting background on related optimization methods.",
561   "evidence": [
562     3
563   ],
564   "pub_time": 2012,
565   "authors": [
566     "Zeiler, Matthew D"
567   ],
568   "source": "arXiv preprint arXiv:1212.5701"

```

```

569 },
570 "Online convex programming and generalized infinitesimal gradient ascent": {
571   "cite_type": "Strong Cite",
572   "related": "The work is a main support for the study's design, as the online
               learning framework proposed in this paper is directly used for the
               convergence analysis.",
573   "evidence": [
574     4
575   ],
576   "pub_time": 2003,
577   "authors": [
578     "Zinkevich, Martin"
579   ]
580 }
581 },
582 "E_Relations": [
583   {
584     "head": "Adam",
585     "head_type": "Method",
586     "relation": "BUILDS_ON",
587     "tail": "AdaGrad",
588     "tail_type": "Method",
589     "evidence": "Our method is designed to combine the advantages of two recently
                  popular methods: AdaGrad (Duchi et al., 2011), which works well with
                  sparse gradients, and RMSProp (Fieleman & Hinton, 2012), which works well
                  in on-line and non-stationary settings",
590     "confidence": "high",
591     "category": "controlled",
592     "source": "semantic"
593   },
594   {
595     "head": "Adam",
596     "head_type": "Method",
597     "relation": "BUILDS_ON",
598     "tail": "RMSProp",
599     "tail_type": "Method",
600     "evidence": "Our method is designed to combine the advantages of two recently
                  popular methods: AdaGrad (Duchi et al., 2011), which works well with
                  sparse gradients, and RMSProp (Fieleman & Hinton, 2012), which works well
                  in on-line and non-stationary settings",
601     "confidence": "high",
602     "category": "controlled",
603     "source": "semantic"
604   },
605   {
606     "head": "Adam",
607     "head_type": "Method",
608     "relation": "SOLVES",
609     "tail": "Stochastic Optimization",
610     "tail_type": "Task",
611     "evidence": "We propose Adam, a method for efficient stochastic optimization
                  that only requires first-order gradients with little memory requirement",
612     "confidence": "high",
613     "category": "controlled",
614     "source": "semantic"
615   },
616   {
617     "head": "Adam",
618     "head_type": "Method",
619     "relation": "USES_TECHNIQUE",
620     "tail": "Bias-Corrected Moment Estimates",
621     "tail_type": "Domain_Term",
622     "evidence": "The method computes individual adaptive learning rates for
                  different parameters from estimates of first and second moments of the
                  gradients",
623     "confidence": "high",
624     "category": "open",
625     "source": "semantic"
626   },
627   {

```

```

628     "head": "Adam",
629     "head_type": "Method",
630     "relation": "REQUIRES",
631     "tail": "first-order gradients",
632     "tail_type": "Requirement",
633     "evidence": "We propose Adam, a method for efficient stochastic optimization
634         that only requires first-order gradients with little memory requirement",
635     "confidence": "high",
636     "category": "open",
637     "source": "semantic"
638 },
639 {
640     "head": "Adam",
641     "head_type": "Method",
642     "relation": "HAS_LIMITATION",
643     "tail": "restricted to first-order methods",
644     "tail_type": "Limitation",
645     "evidence": "discussion in this paper will be restricted to first-order
646         methods",
647     "confidence": "medium",
648     "category": "open",
649     "source": "semantic"
650 },
651 {
652     "head": "Adam",
653     "head_type": "Method",
654     "relation": "USES_TECHNIQUE",
655     "tail": "exponential moving averages",
656     "tail_type": "Technique",
657     "evidence": "The algorithm updates exponential moving averages of the gradient
658         (m_t) and the squared gradient (v_t)",
659     "confidence": "high",
660     "category": "open",
661     "source": "semantic"
662 },
663 {
664     "head": "Adam",
665     "head_type": "Method",
666     "relation": "USES_TECHNIQUE",
667     "tail": "bias-corrected moment estimates",
668     "tail_type": "Domain_Term",
669     "evidence": "this initialization bias can be easily counteracted, resulting in
670         bias-corrected estimates m_hat_t and v_hat_t",
671     "confidence": "high",
672     "category": "open",
673     "source": "semantic"
674 },
675 {
676     "head": "Adam",
677     "head_type": "Method",
678     "relation": "USES_TECHNIQUE",
679     "tail": "adaptive stepsize selection",
680     "tail_type": "Technique",
681     "evidence": "An important property of Adam's update rule is its careful choice
682         of stepsizes",
683     "confidence": "high",
684     "category": "open",
685     "source": "semantic"
686 },
687 {
688     "head": "Adam",
689     "head_type": "Method",
690     "relation": "REQUIRES",
691     "tail": "Signal-to-Noise Ratio (SNR)",
692     "tail_type": "Domain_Term",
693     "evidence": "The stochasticity might come from the evaluation at random
694         subsamples (minibatches) of datapoints, or arise from inherent function
695         noise",
696     "confidence": "medium",
697     "category": "open",

```

```

691     "source": "semantic"
692   },
693   {
694     "head": "Adam",
695     "head_type": "Method",
696     "relation": "USES_COMPONENT",
697     "tail": "Bias-Corrected Moment Estimates",
698     "tail_type": "Domain_Term",
699     "evidence": "Adam utilizes initialization bias correction terms.",
700     "confidence": "high",
701     "category": "controlled",
702     "source": "semantic"
703   },
704   {
705     "head": "Adam",
706     "head_type": "Method",
707     "relation": "USES_TECHNIQUE",
708     "tail": "exponential moving average",
709     "tail_type": "Technique",
710     "evidence": "Adam utilizes initialization bias correction terms.",
711     "confidence": "medium",
712     "category": "open",
713     "source": "semantic"
714   },
715   {
716     "head": "Signal-to-Noise Ratio (SNR)",
717     "head_type": "Domain_Term",
718     "relation": "HAS_PROPERTY",
719     "tail": "bounded by stepsize setting alpha",
720     "tail_type": "Property",
721     "evidence": "The effective magnitude of the steps taken in parameter space at
722     each timestep are approximately bounded by the stepsize setting alpha, i.e
723     .,  $|\Delta_t|$  approximately  $\leq \alpha$ .",
724     "confidence": "high",
725     "category": "open",
726     "source": "semantic"
727   },
728   {
729     "head": "Signal-to-Noise Ratio (SNR)",
730     "head_type": "Domain_Term",
731     "relation": "MODULATES",
732     "tail": "effective stepsize  $\Delta_t$ ",
733     "tail_type": "Property",
734     "evidence": "With a smaller SNR the effective stepsize  $\Delta_t$  will be closer
735     to zero.",
736     "confidence": "high",
737     "category": "open",
738     "source": "semantic"
739   },
740   {
741     "head": "Signal-to-Noise Ratio (SNR)",
742     "head_type": "Domain_Term",
743     "relation": "CORRELATED_WITH",
744     "tail": "uncertainty in gradient direction",
745     "tail_type": "Property",
746     "evidence": "a smaller SNR means that there is greater uncertainty about
747     whether the direction of  $m_{hat}_t$  corresponds to the direction of the true
748     gradient.",
749     "confidence": "high",
750     "category": "open",
751     "source": "semantic"
752   },
753   {
754     "head": "Signal-to-Noise Ratio (SNR)",
755     "head_type": "Domain_Term",
756     "relation": "CORRELATED_WITH",
757     "tail": "automatic annealing",
758     "tail_type": "Process",
759     "evidence": "the SNR value typically becomes closer to 0 towards an optimum,
760     leading to smaller effective steps in parameter space: a form of automatic

```

```

755     annealing.",
756     "confidence": "high",
757     "category": "open",
758     "source": "semantic"
759   },
760   {
761     "head": "effective stepsize Delta_t",
762     "head_type": "Property",
763     "relation": "INHIBITS",
764     "tail": "large parameter updates",
765     "tail_type": "Process",
766     "evidence": "With a smaller SNR the effective stepsize Delta_t will be closer
767     to zero.",
768     "confidence": "medium",
769     "category": "open",
770     "source": "semantic"
771   },
772   {
773     "head": "Adam",
774     "head_type": "Method",
775     "relation": "REQUIRES",
776     "tail": "initialization bias correction",
777     "tail_type": "Requirement",
778     "evidence": "Adam utilizes initialization bias correction terms.",
779     "confidence": "high",
780     "category": "open",
781     "source": "semantic"
782   },
783   {
784     "head": "Bias-Corrected Moment Estimates",
785     "head_type": "Domain_Term",
786     "relation": "IMPLEMENTED_FOR",
787     "tail": "second moment estimate",
788     "tail_type": "Component",
789     "evidence": "We will here derive the term for the second moment estimate; the
790     derivation for the first moment estimate is completely analogous.",
791     "confidence": "medium",
792     "category": "open",
793     "source": "semantic_unknown_type"
794   },
795   {
796     "head": "Bias-Corrected Moment Estimates",
797     "head_type": "Domain_Term",
798     "relation": "REQUIRES",
799     "tail": "stationary true second moment",
800     "tail_type": "Condition",
801     "evidence": "zeta = 0 if the true second moment E[g_t^2] is stationary;
802     otherwise zeta can be kept small since the exponential decay rate beta_1
803     can (and should) be chosen such that the exponential moving average
804     assigns small weights to gradients too far in the past.",
805     "confidence": "medium",
806     "category": "open",
807     "source": "semantic"
808   },
809   {
810     "head": "Adam",
811     "head_type": "Method",
812     "relation": "HAS_LIMITATION",
813     "tail": "large initial steps without bias correction",
814     "tail_type": "Limitation",
815     "evidence": "In case of sparse gradients, for a reliable estimate of the
816     second moment one needs to average over many gradients by choosing a small
817     value of beta_2; however it is exactly this case of small beta_2 where a
818     lack of initialisation bias correction would lead to initial steps that
819     are much larger.",
820     "confidence": "high",
821     "category": "open",
822     "source": "semantic"
823   },
824   },
825   {

```

```

815     "head": "Adam",
816     "head_type": "Method",
817     "relation": "HAS_LIMITATION",
818     "tail": "requires decaying learning rate at  $t^{-1/2}$  and decaying first moment
           coefficient",
819     "tail_type": "Limitation",
820     "evidence": "Our following theorem holds when the learning rate  $\alpha_t$  is
           decaying at a rate of  $t^{-1/2}$  and first moment running average
           coefficient  $\beta_{1,t}$  decay exponentially with  $\lambda$ , that is typically
           close to 1, e.g.  $1-10^{-8}$ .",
821     "confidence": "high",
822     "category": "open",
823     "source": "semantic"
824   },
825   {
826     "head": "Adam",
827     "head_type": "Method",
828     "relation": "REQUIRES",
829     "tail": "bounded gradients of functions",
830     "tail_type": "Requirement",
831     "evidence": "Assume that the function  $f_t$  has bounded gradients,  $\|\nabla f_t(\theta)\|_2 \leq G$ ,  $\|\nabla f_t(\theta)\|_\infty \leq G_\infty$  for all  $\theta$  in  $\mathbb{R}^d$ ",
832     "confidence": "high",
833     "category": "open",
834     "source": "semantic"
835   },
836   {
837     "head": "Adam",
838     "head_type": "Method",
839     "relation": "REQUIRES",
840     "tail": "bounded distance between generated parameters",
841     "tail_type": "Requirement",
842     "evidence": "distance between any  $\theta_t$  generated by Adam is bounded  $\|\theta_n - \theta_m\|_2 \leq D$ ,  $\|\theta_m - \theta_n\|_\infty \leq D_\infty$  for any  $m, n$  in  $\{1, \dots, T\}$ ",
843     "confidence": "high",
844     "category": "open",
845     "source": "semantic"
846   },
847   {
848     "head": "Adam",
849     "head_type": "Method",
850     "relation": "REQUIRES",
851     "tail": " $\beta_1$  and  $\beta_2$  in  $[0, 1)$  satisfying  $\beta_1 / \sqrt{\beta_2} < 1$ ",
852     "tail_type": "Requirement",
853     "evidence": " $\beta_1, \beta_2$  in  $[0, 1)$  satisfy  $\beta_1 / \sqrt{\beta_2} < 1$ ",
854     "confidence": "high",
855     "category": "open",
856     "source": "semantic"
857   },
858   {
859     "head": "Adam",
860     "head_type": "Method",
861     "relation": "ACHIEVES",
862     "tail": " $O(\log d \sqrt{T})$  regret bound",
863     "tail_type": "Metric",
864     "evidence": "adaptive method, such as Adam and Adagrad, can achieve  $O(\log d \sqrt{T})$ ",
865     "confidence": "high",
866     "category": "open",
867     "source": "semantic_unknown_type"
868   },
869   {
870     "head": "Adam",
871     "head_type": "Method",
872     "relation": "IMPROVES_OVER",
873     "tail": "non-adaptive methods with  $O(\sqrt{dT})$  regret bound",
874     "tail_type": "Method",
875     "evidence": "an improvement over  $O(\sqrt{dT})$  for the non-adaptive method",

```

```

876     "confidence": "high",
877     "category": "open",
878     "source": "semantic_unknown_type"
879   },
880   {
881     "head": "Adam",
882     "head_type": "Method",
883     "relation": "USES_TECHNIQUE",
884     "tail": "decaying first moment coefficient beta_1,t",
885     "tail_type": "Technique",
886     "evidence": "Decaying beta_1,t towards zero is important in our theoretical
      analysis",
887     "confidence": "high",
888     "category": "open",
889     "source": "semantic"
890   },
891   {
892     "head": "Adam",
893     "head_type": "Method",
894     "relation": "USES_TECHNIQUE",
895     "tail": "running average of first and second moment of the gradient",
896     "tail_type": "Technique",
897     "evidence": "Adam updates are directly estimated using a running average of
      first and second moment of the gradient.",
898     "confidence": "high",
899     "category": "open",
900     "source": "semantic"
901   },
902   {
903     "head": "RMSProp",
904     "head_type": "Method",
905     "relation": "HAS_LIMITATION",
906     "tail": "lacks bias-correction term",
907     "tail_type": "Limitation",
908     "evidence": "RMSProp also lacks a bias-correction term; this matters most in
      case of a value of beta2 close to 1 (required in case of sparse gradients)
      , since in that case not correcting the bias leads to very large stepsizes
      and often divergence, as we also empirically demonstrate in section 6.4."
909     ,
910     "confidence": "high",
911     "category": "open",
912     "source": "semantic"
913   },
914   {
915     "head": "Adam",
916     "head_type": "Method",
917     "relation": "DIFFERS_FROM",
918     "tail": "RMSProp",
919     "tail_type": "Method",
920     "evidence": "There are a few important differences between RMSProp with
      momentum and Adam: RMSProp with momentum generates its parameter updates
      using a momentum on the rescaled gradient, whereas Adam updates are
      directly estimated using a running average of first and second moment of
      the gradient.",
921     "confidence": "high",
922     "category": "open",
923     "source": "semantic"
924   },
925   {
926     "head": "Adam",
927     "head_type": "Method",
928     "relation": "USES_TECHNIQUE",
929     "tail": "preconditioner that adapts to the geometry of the data",
930     "tail_type": "Technique",
931     "evidence": "Adam employs a preconditioner that adapts to the geometry of the
      data, since v_hat_t is an approximation to the diagonal of the Fisher
      information matrix (Pascanu & Bengio, 2013);",
932     "confidence": "high",
933     "category": "open",
934     "source": "semantic"

```

```

934 },
935 {
936   "head": "Adam",
937   "head_type": "Method",
938   "relation": "DERIVED_FROM",
939   "tail": "natural gradient descent",
940   "tail_type": "Method",
941   "evidence": "Like natural gradient descent (NGD) (Amari, 1998), Adam employs a
    preconditioner that adapts to the geometry of the data, since  $\hat{v}_t$  is
    an approximation to the diagonal of the Fisher information matrix (Pascanu
    & Bengio, 2013);",
942   "confidence": "high",
943   "category": "open",
944   "source": "semantic"
945 },
946 {
947   "head": "AdaGrad",
948   "head_type": "Method",
949   "relation": "BUILDS_ON",
950   "tail": "Adam",
951   "tail_type": "Method",
952   "evidence": "AdaGrad corresponds to a version of Adam with  $\beta_1=0$ ,
    infinitesimal  $(1-\beta_2)$  and a replacement of alpha by an annealed version
     $\alpha_t = \alpha * t^{-1/2}$ ",
953   "confidence": "high",
954   "category": "controlled",
955   "source": "semantic"
956 },
957 {
958   "head": "AdaGrad",
959   "head_type": "Method",
960   "relation": "ALTERNATIVE_TO",
961   "tail": "RMSProp",
962   "tail_type": "Method",
963   "evidence": "Note that this direct correspondence between Adam and Adagrad
    does not hold when removing the bias-correction terms; without bias
    correction, like in RMSProp, a  $\beta_2$  infinitesimally close to 1 would lead
    to infinitely large bias",
964   "confidence": "high",
965   "category": "controlled",
966   "source": "semantic"
967 },
968 {
969   "head": "RMSProp",
970   "head_type": "Method",
971   "relation": "HAS_LIMITATION",
972   "tail": "Infinitely Large Bias",
973   "tail_type": "Limitation",
974   "evidence": "without bias correction, like in RMSProp, a  $\beta_2$  infinitesimally
    close to 1 would lead to infinitely large bias",
975   "confidence": "high",
976   "category": "open",
977   "source": "semantic"
978 },
979 {
980   "head": "Adam",
981   "head_type": "Method",
982   "relation": "REQUIRES",
983   "tail": "Bias-Corrected Moment Estimates",
984   "tail_type": "Domain_Term",
985   "evidence": "Note that this direct correspondence between Adam and Adagrad
    does not hold when removing the bias-correction terms",
986   "confidence": "high",
987   "category": "open",
988   "source": "semantic"
989 },
990 {
991   "head": "AdaGrad",
992   "head_type": "Method",
993   "relation": "BUILDS_ON",

```

```

994     "tail": "Stochastic Optimization",
995     "tail_type": "Task",
996     "evidence": "Adagrad can efficiently deal with sparse features and gradients
          as one of its main theoretical results whereas SGD is low at learning rare
          features.",
997     "confidence": "high",
998     "category": "controlled",
999     "source": "semantic"
1000   },
1001   {
1002     "head": "Adam",
1003     "head_type": "Method",
1004     "relation": "BUILDS_ON",
1005     "tail": "Stochastic Optimization",
1006     "tail_type": "Task",
1007     "evidence": "Adam with  $1/\sqrt{t}$  decay on its stepsize should
          theoretically match the performance of Adagrad.",
1008     "confidence": "high",
1009     "category": "controlled",
1010     "source": "semantic"
1011   },
1012   {
1013     "head": "Adam",
1014     "head_type": "Method",
1015     "relation": "USES_TECHNIQUE",
1016     "tail": " $1/\sqrt{t}$  stepsize decay",
1017     "tail_type": "Technique",
1018     "evidence": "Adam with  $1/\sqrt{t}$  decay on its stepsize should
          theoretically match the performance of Adagrad.",
1019     "confidence": "high",
1020     "category": "open",
1021     "source": "semantic"
1022   },
1023   {
1024     "head": "Adam",
1025     "head_type": "Method",
1026     "relation": "CONSISTS_OF",
1027     "tail": "Bias-Corrected Moment Estimates",
1028     "tail_type": "Domain_Term",
1029     "evidence": "Similar to Adagrad, Adam can take advantage of sparse features
          and obtain faster convergence rate than normal SGD with momentum.",
1030     "confidence": "medium",
1031     "category": "open",
1032     "source": "semantic"
1033   },
1034   {
1035     "head": "SFO",
1036     "head_type": "Method",
1037     "relation": "REQUIRES",
1038     "tail": "deterministic subfunctions",
1039     "tail_type": "Requirement",
1040     "evidence": "SFO assumes deterministic subfunctions, and indeed failed to
          converge on cost functions with stochastic regularization.",
1041     "confidence": "high",
1042     "category": "open",
1043     "source": "semantic"
1044   },
1045   {
1046     "head": "SFO",
1047     "head_type": "Method",
1048     "relation": "HAS_LIMITATION",
1049     "tail": "incompatibility with stochastic regularization",
1050     "tail_type": "Limitation",
1051     "evidence": "SFO assumes deterministic subfunctions, and indeed failed to
          converge on cost functions with stochastic regularization.",
1052     "confidence": "high",
1053     "category": "open",
1054     "source": "semantic"
1055   },
1056   {

```

```

1057     "head": "Adam",
1058     "head_type": "Method",
1059     "relation": "USES_TECHNIQUE",
1060     "tail": "dropout noise",
1061     "tail_type": "Technique",
1062     "evidence": "Adam shows better convergence than other methods on multi-layer
1063         neural networks trained with dropout noise.",
1064     "confidence": "medium",
1065     "category": "open",
1066     "source": "semantic"
1067 },
1068 {
1069     "head": "Adagrad",
1070     "head_type": "Method",
1071     "relation": "HAS_LIMITATION",
1072     "tail": "vanishing second moment estimate in CNNs",
1073     "tail_type": "Limitation",
1074     "evidence": "The second moment estimate  $\widehat{v}_t$  vanishes to zeros
1075         after a few epochs and is dominated by the  $\epsilon$  in algorithm 1.",
1076     "confidence": "high",
1077     "category": "open",
1078     "source": "semantic"
1079 },
1080 {
1081     "head": "Adam",
1082     "head_type": "Method",
1083     "relation": "REQUIRES",
1084     "tail": "bias correction term for robustness to sparse gradients",
1085     "tail_type": "Requirement",
1086     "evidence": "Values of  $\beta_2$  close to 1, required for robustness to
1087         sparse gradients, results in larger initialization bias; therefore we
1088         expect the bias correction term is important in such cases of slow decay,
1089         preventing an adverse effect on optimization.",
1090     "confidence": "high",
1091     "category": "open",
1092     "source": "semantic"
1093 },
1094 {
1095     "head": "Adam",
1096     "head_type": "Method",
1097     "relation": "COMBINES",
1098     "tail": "first moment variance reduction with second moment estimation",
1099     "tail_type": "Technique",
1100     "evidence": "Whereas, reducing the minibatch variance through the first moment
1101         is more important in CNNs and contributes to the speed-up.",
1102     "confidence": "medium",
1103     "category": "open",
1104     "source": "semantic"
1105 },
1106 {
1107     "head": "Adam",
1108     "head_type": "Method",
1109     "relation": "DERIVED_FROM",
1110     "tail": "RMSProp",
1111     "tail_type": "Method",
1112     "evidence": "Discussed in section 5, removal of the bias correction terms
1113         results in a version of RMSProp (Tieleman & Hinton, 2012) with momentum.",
1114     "confidence": "high",
1115     "category": "open",
1116     "source": "semantic"
1117 },
1118 {
1119     "head": "Adam",
1120     "head_type": "Method",
1121     "relation": "USES_TECHNIQUE",
1122     "tail": "bias correction in moment estimates",
1123     "tail_type": "Technique",
1124     "evidence": "Values of  $\beta_2$  close to 1, required for robustness to
1125         sparse gradients, results in larger initialization bias; therefore we
1126         expect the bias correction term is important in such cases of slow decay,

```

```

    preventing an adverse effect on optimization.",
1118   "confidence": "high",
1119   "category": "open",
1120   "source": "semantic"
1121 },
1122 {
1123   "head": "AdaMax",
1124   "head_type": "Method",
1125   "relation": "BUILDS_ON",
1126   "tail": "Adam",
1127   "tail_type": "Method",
1128   "evidence": "AdaMax, a variant of Adam based on the infinity norm.",
1129   "confidence": "high",
1130   "category": "controlled",
1131   "source": "semantic"
1132 },
1133 {
1134   "head": "AdaMax",
1135   "head_type": "Method",
1136   "relation": "USES_TECHNIQUE",
1137   "tail": "infinity norm",
1138   "tail_type": "Technique",
1139   "evidence": "AdaMax, a variant of Adam based on the infinity norm.",
1140   "confidence": "high",
1141   "category": "open",
1142   "source": "semantic"
1143 },
1144 {
1145   "head": "Adam",
1146   "head_type": "Method",
1147   "relation": "USES_TECHNIQUE",
1148   "tail": "L2 norm",
1149   "tail_type": "Technique",
1150   "evidence": "In Adam, the update rule for individual weights is to scale their
    gradients inversely proportional to a (scaled)  $L^2$  norm of their
    individual current and past gradients.",
1151   "confidence": "high",
1152   "category": "open",
1153   "source": "semantic"
1154 },
1155 {
1156   "head": "AdaMax",
1157   "head_type": "Method",
1158   "relation": "REQUIRES",
1159   "tail": "bias-correction term",
1160   "tail_type": "Technique",
1161   "evidence": "( $\alpha/(1-\beta_{1}^t)$ ) is the learning rate with the bias
    -correction term for the first moment.",
1162   "confidence": "high",
1163   "category": "open",
1164   "source": "semantic"
1165 },
1166 {
1167   "head": "Adam",
1168   "head_type": "Method",
1169   "relation": "REQUIRES",
1170   "tail": "bias-correction term",
1171   "tail_type": "Technique",
1172   "evidence": "The best results were achieved with small values of  $(1-\beta_{2}^t)$ 
    and bias correction;",
1173   "confidence": "high",
1174   "category": "open",
1175   "source": "semantic"
1176 },
1177 {
1178   "head": "Adam",
1179   "head_type": "Method",
1180   "relation": "HAS_LIMITATION",
1181   "tail": "instability without bias correction",
1182   "tail_type": "Limitation",

```

```

1183     "evidence": "values  $\beta_{2}$  close to 1 indeed lead to instabilities in
1184         training when no bias correction term was present",
1185     "confidence": "high",
1186     "category": "open",
1187     "source": "semantic"
1188   },
1189   {
1190     "head": "AdaMax",
1191     "head_type": "Method",
1192     "relation": "HAS_LIMITATION",
1193     "tail": "Initialization bias",
1194     "tail_type": "Limitation",
1195     "evidence": "Initialization bias can again be corrected by the estimator",
1196     "confidence": "medium",
1197     "category": "open",
1198     "source": "semantic"
1199   },
1200   {
1201     "head": "AdaMax",
1202     "head_type": "Method",
1203     "relation": "USES_TECHNIQUE",
1204     "tail": "exponential moving average",
1205     "tail_type": "Technique",
1206     "evidence": "an exponential moving average over the parameters can be used",
1207     "confidence": "high",
1208     "category": "open",
1209     "source": "semantic"
1210   },
1211   {
1212     "head": "AdaMax",
1213     "head_type": "Method",
1214     "relation": "REQUIRES",
1215     "tail": "parameter initialization",
1216     "tail_type": "Requirement",
1217     "evidence": "with initial value  $u_{0} = 0$ ",
1218     "confidence": "medium",
1219     "category": "open",
1220     "source": "semantic"
1221   },
1222   {
1223     "head": "AdaMax",
1224     "head_type": "Method",
1225     "relation": "DERIVED_FROM",
1226     "tail": "Adam",
1227     "tail_type": "Method",
1228     "evidence": "the magnitude of parameter updates has a simpler bound with
1229         AdaMax than Adam",
1230     "confidence": "high",
1231     "category": "open",
1232     "source": "semantic"
1233   },
1234   {
1235     "head": "AdaMax",
1236     "head_type": "Method",
1237     "relation": "USES_TECHNIQUE",
1238     "tail": "recursive formula",
1239     "tail_type": "Technique",
1240     "evidence": "Which corresponds to the remarkably simple recursive formula",
1241     "confidence": "high",
1242     "category": "open",
1243     "source": "semantic"
1244   },
1245   {
1246     "head": "AdaMax",
1247     "head_type": "Method",
1248     "relation": "HAS_LIMITATION",
1249     "tail": "noisy last iterate",
1250     "tail_type": "Limitation",
1251     "evidence": "Since the last iterate is noisy due to stochastic approximation",
1252     "confidence": "medium",
  
```

```

1251     "category": "open",
1252     "source": "semantic"
1253   },
1254   {
1255     "head": "AdaMax",
1256     "head_type": "Method",
1257     "relation": "USES_TECHNIQUE",
1258     "tail": "Polyak-Ruppert averaging",
1259     "tail_type": "Technique",
1260     "evidence": "Previously in Moulines & Bach (2011), Polyak-Ruppert averaging
1261       has been shown to improve the convergence of standard SGD",
1262     "confidence": "medium",
1263     "category": "open",
1264     "source": "semantic"
1265   },
1266   {
1267     "head": "AdaMax",
1268     "head_type": "Method",
1269     "relation": "USES_TECHNIQUE",
1270     "tail": "exponential moving average estimator",
1271     "tail_type": "Technique",
1272     "evidence": "Initialization bias can again be corrected by the estimator  $\widehat{\theta}_t = \widehat{\theta}_t / (1 - \beta_2^t)$ ",
1273     "confidence": "medium",
1274     "category": "open",
1275     "source": "semantic"
1276   },
1277   {
1278     "head": "Adam",
1279     "head_type": "Method",
1280     "relation": "APPLIED_TO",
1281     "tail": "non-convex optimization problems",
1282     "tail_type": "Task",
1283     "evidence": "we found Adam to be robust and well-suited to a wide range of non
1284       -convex optimization problems in the field machine learning",
1285     "confidence": "high",
1286     "category": "controlled",
1287     "source": "semantic"
1288   },
1289   {
1290     "head": "Adam",
1291     "head_type": "Method",
1292     "relation": "REQUIRES",
1293     "tail": "little memory",
1294     "tail_type": "Requirement",
1295     "evidence": "The method is straightforward to implement and requires little
1296       memory",
1297     "confidence": "high",
1298     "category": "open",
1299     "source": "semantic"
1300   },
1301   {
1302     "head": "Adam",
1303     "head_type": "Method",
1304     "relation": "REQUIRES",
1305     "tail": "computationally efficient algorithm",
1306     "tail_type": "Requirement",
1307     "evidence": "We have introduced a simple and computationally efficient
1308       algorithm for gradient-based optimization of stochastic objective
1309       functions",
1310     "confidence": "medium",
1311     "category": "open",
1312     "source": "semantic"
1313   }
1314 ],
1315 "entity_aliases": {
1316   "adaptive moment estimation": "Adam",
1317   "Adam optimizer": "Adam",
1318   "Adaptive Gradient Algorithm": "AdaGrad",
1319   "Root Mean Square Propagation": "RMSProp",

```

```
1315 "Adaptive Moment Estimation with Infinity Norm": "AdaMax",
1316 "stochastic gradient descent": "Stochastic Optimization",
1317 "adaptive optimization": "Stochastic Optimization",
1318 "Regret": "Regret Bound",
1319 "SNR": "Signal-to-Noise Ratio (SNR)",
1320 "Bias Correction": "Bias-Corrected Moment Estimates"
1321 }
1322 }
```